



HAL
open science

Genetic Diversity of Collaborative Cross Mice Controls Viral Replication, Clinical Severity, and Brain Pathology Induced by Zika Virus Infection, Independently of Oas1b

Caroline Manet, Etienne Simon-Loriere, Grégory Jouvion, David Hardy, Matthieu Prot, Laurine Conquet, Marie Flamand, Jean-Jacques Panthier, Anavaj Sakuntabhai, Xavier Montagutelli

► To cite this version:

Caroline Manet, Etienne Simon-Loriere, Grégory Jouvion, David Hardy, Matthieu Prot, et al.. Genetic Diversity of Collaborative Cross Mice Controls Viral Replication, Clinical Severity, and Brain Pathology Induced by Zika Virus Infection, Independently of Oas1b. *Journal of Virology*, 2020, 94 (3), 10.1128/JVI.01034-19 . hal-02445236

HAL Id: hal-02445236

<https://hal.science/hal-02445236v1>

Submitted on 20 Jan 2020

HAL is a multi-disciplinary open access archive for the deposit and dissemination of scientific research documents, whether they are published or not. The documents may come from teaching and research institutions in France or abroad, or from public or private research centers.

L'archive ouverte pluridisciplinaire **HAL**, est destinée au dépôt et à la diffusion de documents scientifiques de niveau recherche, publiés ou non, émanant des établissements d'enseignement et de recherche français ou étrangers, des laboratoires publics ou privés.

1 **Title: Genetic diversity of Collaborative Cross mice controls viral replication,**
2 **clinical severity and brain pathology induced by Zika virus infection,**
3 **independently of *Oas1b*.**

4 Running title: Host genetic susceptibility to Zika virus disease

5 Caroline Manet,^a Etienne Simon-Lorière,^b Grégory Jouvion,^{c,d} David Hardy,^d Matthieu Prot,^b

6 Laurine Conquet,^a Marie Flamand,^c Jean-Jacques Panthier,^a Anavaj Sakuntabhai,^f Xavier

7 Montagutelli^{a#}

8 **Affiliations:**

9 ^a Mouse Genetics Laboratory, Department of Genomes and Genetics, Institut Pasteur, 75015
10 Paris, France

11 ^b Evolutionary Genomics of RNA Viruses, Department of Virology, Institut Pasteur, 75015
12 Paris, France

13 ^c Sorbonne Université, INSERM, Pathophysiology of Pediatric Genetic Diseases, AP-HP,
14 Hôpital Armand-Trousseau, UF de Génétique Moléculaire, 75012 Paris, France

15 ^d Institut Pasteur, Experimental Neuropathology Unit, Department of Global Health, 75015 Paris,
16 France

17 ^e Structural Virology Unit, Department of Virology, CNRS UMR 3569, Institut Pasteur, 75015
18 Paris, France

19 ^f Functional Genetics of Infectious Diseases Unit, Department of Global Health, Institut Pasteur,
20 CNRS UMR 2000, 75015 Paris, France

21
22 #Address correspondence to Xavier Montagutelli, xavier.montagutelli@pasteur.fr

23 **Word counts:** Abstract: 226 - Text: 8410

24

25 **ABSTRACT**

26 The explosive spread of Zika virus (ZIKV) has been associated with major variations in severe
27 disease and congenital afflictions among infected populations, suggesting an influence of host
28 genes. We investigated how genome-wide variants could impact susceptibility to ZIKV infection
29 in mice. We first describe that the susceptibility of *Ifnar1* knockout mice is largely influenced by
30 their genetic background. We then show that the broad genetic diversity of Collaborative Cross
31 mice, of which receptor to type I interferon (IFNAR) was blocked by anti-IFNAR antibody,
32 expressed phenotypes ranging from complete resistance to severe symptoms and death with large
33 variations in the peak and rate of decrease of plasma viral load, in brain viral load, in brain
34 histopathology and in viral replication rate in infected cells. Differences in susceptibility between
35 CC strains were correlated between Zika, Dengue and West Nile viruses. We identified highly
36 susceptible and resistant mouse strains as new models to investigate the mechanisms of human
37 ZIKV disease and other flavivirus infections. Genetic analyses revealed that phenotypic
38 variations are driven by multiple genes with small effects, reflecting the complexity of ZIKV
39 disease susceptibility in human population. Notably, our results rule out a role of the *Oas1b* gene
40 in the susceptibility to ZIKV. Altogether, this study emphasizes the role of host genes in the
41 pathogeny of ZIKV infection and lays the foundation for further genetic and mechanistic studies.

42

43 **IMPORTANCE**

44 In recent outbreaks, ZIKV has infected millions of people and induced rare but potentially severe
45 complications, including Guillain-Barré syndrome and encephalitis in adults. While several viral

46 sequence variants were proposed to enhance the pathogenicity of ZIKV, the influence of host
47 genetic variants in mediating the clinical heterogeneity remains mostly unexplored. We have
48 addressed this question using a mouse panel which models the genetic diversity of human
49 population and a ZIKV strain from a recent clinical isolate. Through a combination of *in vitro*
50 and *in vivo* approaches, we demonstrate that multiple host genetic variants determine viral
51 replication in infected cells, and clinical severity, kinetics of blood viral load and brain pathology
52 in mice. We describe new mouse models expressing high susceptibility or resistance to ZIKV
53 and to other flaviviruses. These models will facilitate the identification and mechanistic
54 characterization of host genes that influence ZIKV pathogenesis.

55

56 **KEYWORDS**

57 Zika virus, flavivirus, mouse model, host genetics, genetic diversity, Collaborative Cross

58

59

60 Zika virus (ZIKV) is a mosquito-borne flavivirus isolated in 1947 from a febrile rhesus
61 monkey in Uganda (1). Until 2007, ZIKV had circulated in Africa and Asia causing mild flu-like
62 syndromes, with rare reported clinical cases (2). However, during recent epidemics, ZIKV
63 infection triggered severe complications including Guillain-Barré syndrome and encephalitis in
64 adults (3, 4), and congenital malformations in fetuses of infected pregnant women (5, 6). Viral
65 mutations may have contributed to ZIKV enhanced pathogenicity (7, 8) but only partly explain
66 the variable proportion of symptomatic infections between populations (9) and the increased
67 incidence of congenital Zika syndrome (CZS) in Polynesia (10) and Brazil (11), suggesting a
68 role for host genetic variants. Recent evidence indicates that the regulation of innate immunity
69 genes is driven by host genetic background in human fetal brain-derived neural stem cells
70 (hNSCs) infected *in vitro* with ZIKV (12). Additionally, the analysis of pairs of dizygotic twins
71 exposed to ZIKV during pregnancy and discordant for CZS suggests multigenic host
72 susceptibility to ZIKV-induced brain malformations (13).

73 Multiple mouse models have been proposed to decipher the mechanisms of ZIKV disease
74 pathogenesis (14, 15). These models allow the investigation of several key features of human
75 infection, such as neuronal damage (16, 17), sexual and vertical transmission (18-21), fetal
76 demise and CZS (22-25). However, while non-structural ZIKV proteins efficiently inhibit innate
77 antiviral responses in humans (26, 27) allowing viral replication, ZIKV replicates poorly in wild-
78 type mice due to the inability of its NS5 protein to antagonize STAT2 and type I interferon (IFN)
79 response as in humans (28). Effective systemic infection in mice occurs when this response is
80 abrogated by genetic inactivation of the *Ifnar1* gene (29) or by blocking the type I IFN receptor
81 with the MAR1-5A3 monoclonal antibody (mAb) (30, 31). So far, host genetic factors involved
82 in mouse susceptibility to ZIKV infection have been investigated mainly through reverse genetic
83 approaches, by studying the consequences of genetic ablation of specific genes, such as innate or

84 adaptive immunity genes (29, 32-35). While these models have contributed to our understanding
85 of the mechanisms of ZIKV disease, they do not model the simultaneous contribution of variants
86 in multiple pathways, as would most likely be observed in the natural population. A recent study
87 has reported strain-specific differences in the susceptibility to neonatal ZIKV infection across
88 four mouse laboratory strains, affecting neuropathology and behavior in adulthood (36). More
89 extensive studies investigating the role of genome-wide genetic variations on the susceptibility to
90 ZIKV infection are needed, using mouse models that reflect the phenotypic and genetic diversity
91 of the human population (37).

92 In this study, we addressed this question using two types of susceptible mouse models.
93 First, since the phenotype of a single gene modification often varies under the influence of
94 modifier genes (38, 39), we assessed the effect of host genetic background on the susceptibility
95 of *Ifnar1*-deficient mice. We then investigated the impact of host genetic diversity on the
96 susceptibility to ZIKV infection in the Collaborative Cross (CC), a panel of recombinant inbred
97 mice produced via a funnel breeding scheme that combined eight founder inbred strains,
98 including five classic laboratory strains and three wild-derived strains (40). As a result, every CC
99 strains has inherited a unique and balanced contribution for each of the eight founder strains.
100 These founder strains capture approximately 90% of the genetic variants present in the *Mus*
101 *musculus* species (41) and the resulting CC strains, which segregate an estimated 45 million
102 polymorphisms, have more genetic diversity than the human population (42). Extensive
103 variations in pathogenic phenotypes have been previously reported in the CC panel after viral
104 (43-50), bacterial (51, 52) and fungal (53) infections, demonstrating that this resource is ideally
105 suited for investigating the role of host genetic variants in the pathophysiology of infectious
106 diseases (54).

107 Susceptibility to ZIKV in *Ifnar1*-deficient mice was strongly influenced by the genetic
108 background, which has practical implications for future virology studies to identify modifier
109 genes. The challenge of 35 immunocompetent CC strains with ZIKV after MAR1-5A3 mAb
110 treatment allowed efficient viral replication. We show that genetic diversity in the CC panel
111 enabled large variations in the clinical severity of ZIKV disease, in the peak and kinetics of
112 plasma viral load and in the severity of ZIKV-induced brain pathology. Genetic diversity also
113 resulted in differences in the permissiveness of CC mouse cells to viral replication which likely
114 contributes to the *in vivo* phenotypic range. In a subset of CC strains, we found correlated
115 differences of susceptibility to ZIKV, dengue virus (DENV) and West Nile virus (WNV),
116 suggesting shared underlying mechanisms. We identified highly susceptible and resistant mouse
117 strains as new models to investigate the mechanisms of human ZIKV disease and other flavivirus
118 infections. Finally, genetic analysis revealed that susceptibility to ZIKV in the CC is driven by
119 multiple loci with small individual effects, and that *Oas1b*, a major determinant of mouse
120 susceptibility to WNV, is not involved.

121

122 **RESULTS**

123 **Genetic background controls the susceptibility of *Ifnar1*-deficient mice to ZIKV**

124 Many studies have used *Ifnar1* knock-out mice on 129S2/SvPas (129) (55, 56) or C57BL/6J
125 (B6) (23, 29, 34) inbred backgrounds, but the differences in ZIKV susceptibility between these
126 two strains have not been reported and remain unclear due to heterogeneous experimental
127 conditions between studies. We compared the susceptibility of age-matched 129S2/SvPas-*Ifnar1*^{-/-}
128 (129-*Ifnar1*) and C57BL/6J-*Ifnar1*^{-/-} (B6-*Ifnar1*) mice infected intraperitoneally (IP) with 10⁷
129 FFUs of FG15 ZIKV. B6-*Ifnar1* mice showed increasingly severe symptoms, with body weight
130 loss, ruffled fur, ataxia and hind limb paralysis from day 4 p.i. and were all (10/10) moribund or
131 dead by day 7 p.i. By contrast, 129-*Ifnar1* mice developed mild symptoms (ruffled fur, hunched
132 back) starting on day 6 p.i. and declining over the second week of infection, with one mouse
133 dying on day 9 p.i. (Fig. 1), demonstrating that the susceptibility to ZIKV infection conferred by
134 *Ifnar1* genetic inactivation is critically influenced by the host genetic background.

135 **mAb blockade of IFNAR is a robust model to study ZIKV infection in CC mice**

136 *Ifnar1* genetic deficiency permanently abrogates IFN- α/β -mediated immune responses but is
137 not currently available on diverse genetic backgrounds. We therefore tested the suitability of
138 transient IFNAR blockade mediated by mAb treatment as a model to study ZIKV infection in
139 genetically diverse mice like the CC. Since MAR1-5A3 mAb was generated in a laboratory
140 strain (129-*Ifnar1* mice) (30) and since the CC strains differ in their *Ifnar1* allele (Table 1), we
141 first compared the coding sequence of the *Ifnar1* gene across the eight founder strains. While
142 129S1/SvImJ, NOD/ShiLtJ, NZO/HiLtJ and WSB/EiJ mice carry the same *Ifnar1* allele as
143 C57BL/6J, A/J, PWK/PhJ and CAST/EiJ mice differ by one, three and seven amino-acids from
144 the C57BL/6J reference sequence, respectively (Table 2). Notably, all three PWK/PhJ variants

145 were found in CAST/EiJ. Therefore, we assessed the efficacy of the MAR1-5A3 mAb by
146 Western Blot analysis on mouse embryonic fibroblasts (MEFs) isolated from two CC strains
147 (CC001 and CC071) both of which inherited the *Ifnar1* allele from the most divergent CAST/EiJ
148 strain (57), by comparison with B6 MEFs. IFNAR stimulation by IFN- α/β activates the
149 JAK1/TYK2 pathway and results in the phosphorylation of STAT1. We found that, in B6,
150 CC001 and CC071 MEFs, STAT1 phosphorylation was equally induced by murine IFN- α and
151 fully inhibited by the MAR1-5A3 mAb (Fig. 2A).

152 To assess MAR1-5A3 mAb efficacy *in vivo*, we infected CC001 and CC071 strains with 10^7
153 FFUs of FG15 ZIKV IP and we measured the kinetics of plasma viral load in mice with and
154 without 2 mg mAb treatment 24 hours prior to infection. Consistent with previous studies in B6
155 (31, 58) and BALB/c (59) mice, viral load was consistently 4 to 5 \log_{10} units higher in mAb-
156 treated mice of both CC001 and CC071 strains compared to untreated mice, demonstrating that
157 MAR1-5A3 mAb treatment successfully increases CC mouse permissiveness to ZIKV
158 replication (Fig. 2B).

159 We then measured the kinetics of plasma viral load in 129-*Ifnar1* strain as well as in four
160 mAb-treated CC strains infected with 10^7 FFUs of FG15 ZIKV IP. We established that the peak
161 plasma viral load occurred in most individuals at day 2 p.i., independently of mouse genetic
162 background (Fig. 2C).

163 In previous studies, viral loads have been measured either by FFU titration or by RT-qPCR
164 quantification of viral genome copies. We compared these two methods in B6-*Ifnar1*, 129-
165 *Ifnar1*, and in ten mAb-treated CC strains (Fig. 2D). We performed Focus Forming Assays
166 (FFA) to measure viral particles in the plasma at day 2 p.i. and confirmed the production of
167 infectious ZIKV in the blood of all strains. Next, we compared the plasma viral load measured

168 by RT-qPCR and by FFA. We found that these two parameters were strongly correlated over a 2
169 \log_{10} range (Pearson coefficient, $r^2=0.89$, $p=9.9 \times 10^{-17}$), with the number of genome copies being
170 on average 3 \log_{10} units higher than the number of FFUs (Fig. 2D). We therefore validated that
171 RT-qPCR measurement of plasma viral load could be used as a labor-efficient proxy for viremia
172 throughout the study.

173 Finally, we compared plasma viral load at day 2 p.i. between males and females in 129-
174 *Ifnar1* and in four mAb-treated CC strains in which both sexes had been tested. We found no
175 significant difference between sexes across diverse genetic backgrounds (two-way ANOVA,
176 $p=0.24$; Fig. 2E), validating the use of merged data from males and females in mouse ZIKV
177 infection experiments.

178 **CC genetic diversity drives ZIKV disease severity and plasma viral load**

179 To explore broad genetic variation, we assessed the susceptibility of mAb-treated mice of 35
180 CC strains. B6-*Ifnar1*, 129-*Ifnar1* and mAb-treated B6 mice were included as reference strains.
181 Only mice from three CC strains developed symptoms as shown on Fig. 3A which summarizes
182 clinical observations at day 7 p.i. CC021 and CC026 mice recovered and survived, while
183 symptoms worsened in 7/9 (78%) CC071 mice which were moribund or died between days 7 and
184 9 p.i.

185 Plasma viral load was measured on days 2 and 6 p.i. At day 2 p.i., which corresponds to its
186 peak, viral load was generally characterized by small within-strain heterogeneity and large inter-
187 strain variations spread over a 2.8 \log_{10} range (Fig. 3B), demonstrating a strong effect of host
188 genes (Kruskal-Wallis, $p=4.8 \times 10^{-15}$) with a broad sense heritability of 86% (60). The three
189 symptomatic CC strains showed the highest peak viral load, close to that of B6-*Ifnar1* and 129-
190 *Ifnar1* mice. However, other strains (such as CC005 and CC061) had similarly high viral loads
191 but never showed any clinical signs of disease, indicating that peak viral load is unlikely the sole

192 factor controlling clinical severity. At day 6 p.i., within-strain variations were larger and more
193 heterogeneous, but we still observed highly significant inter-strain differences (Kruskal-Wallis,
194 $p=1.1 \times 10^{-10}$). Interestingly, viral load on days 2 and 6 p.i. were only moderately correlated
195 (Pearson coefficient, $r^2=0.46$; $p=0.004$), indicating that viral load at day 2 p.i. was not predictive
196 of viral load at day 6 p.i. (see for example CC018 and CC040, or CC026 and CC071).

197 We used the difference of the \log_{10} plasma viral loads between days 2 and 6 p.i. to estimate
198 the clearance rate of the virus from the blood stream (Fig. 3C; the order of the strains sorted by
199 increasing clearance rate was therefore different from those in Fig. 3A and 3B). This rate varied
200 over a 3.3 \log_{10} range between strains, demonstrating a strong effect of host genes (Kruskal-
201 Wallis, $p=2.2 \times 10^{-12}$) with a broad sense heritability of 76%. B6-*Ifnar1* mice showed a slower
202 decrease in viral load than 129-*Ifnar1* mice (Wilcoxon, $p=1.7 \times 10^{-5}$), despite similar peak viral
203 load at day 2 p.i. To confirm that differences between CC strains were not due to differential
204 rates of MAR1-5A3 antibody turnover, we treated CC012 (which showed 4.4 log decrease) and
205 CC037 (1.9 log decrease) with 2 mg of mAb 24 hours before ZIKV infection, with or without
206 two additional injections of 1 mg on days 2 and 4 post-infection. No differences in plasma viral
207 load on days 2 and 6 p.i. were observed between the two conditions (Fig. 2F).

208 Overall, genetic diversity in the CC panel controlled clinical severity of ZIKV infection,
209 mouse survival, and the peak and clearance rate of plasma viral load. Of note, there was no
210 association, across the 35 CC strains tested, between the peak plasma viral load and the *Ifnar1*
211 allele inherited from the founder strain (ANOVA, $p>0.09$). This analysis confirms our *in vitro*
212 data (Fig. 2A) and indicates that the variations in peak plasma viral load do not result from
213 differences in mAb treatment efficacy due to the mAb turnover or to the *Ifnar1* alleles.

214 From this screening, we identified several strains with extreme phenotypes, in particular
215 CC071 which was the most susceptible to ZIKV infection, CC001, CC011, CC017 or CC060

216 with low peak plasma viral load, CC040 with slowly decreasing plasma viral load and CC045 or
217 CC026 with high peak but fast-decreasing plasma viral loads.

218 **CC mice show correlated susceptibility to ZIKV, DENV and WNV**

219 We further characterized three CC strains (indicated by arrows on Fig. 3B and Fig. 3C)
220 among those showing lowest (CC001) and highest peak viral loads with (CC071) or without
221 (CC005) clinical symptoms. To establish whether the above differences were specific of the
222 FG15 ZIKV strain of the Asian lineage, we first assessed the susceptibility of the three selected
223 strains to the HD78788 ZIKV strain of the African lineage. 129-*Ifnar1* mice and mAb-treated
224 CC mice were infected with 10^3 FFUs of HD78788 ZIKV IP which proved to be highly
225 pathogenic in *Ifnar1*-deficient mice with rapid and severe symptoms and 100% mortality (Fig.
226 4A). CC001 was fully resistant with no or mild clinical signs (Fig. 4A, left and center panels).
227 By contrast, all CC071 mice were moribund or dead by day 10 p.i., with early and quickly
228 aggravating symptoms, almost like 129-*Ifnar1* mice. Only one of the 5 CC005 mice developed
229 symptoms and died. Peak viral load (day 2 p.i.) varied over a 2.4 \log_{10} range and the differences
230 between strains were similar to those observed with the FG15 ZIKV strain (Fig. 3B). Here again,
231 plasma viral load at day 2 p.i. was the highest in the very susceptible CC071 and 129-*Ifnar1*
232 strains and low in the resistant CC001, but it was also very high in CC005 mice which were
233 moderately susceptible, confirming that clinical severity does not depend solely on peak plasma
234 viral load.

235 To evaluate whether these differences in susceptibility were specific to ZIKV or extended to
236 other flaviviruses, we assessed the phenotype of a few strains after infection with DENV and
237 WNV, two other members of the *Flaviridae* family.

238 We measured plasma viral load after IV infection with 2×10^6 FFUs of KDH0026A DENV
239 (DENV 1 serotype) in mAb-treated CC001, CC071 and B6 mice and in 129-*Ifnar1* and B6-

240 *Ifnar1* mice (Fig. 4B right). Most inter-strain differences observed with ZIKV FG15 strain (Fig.
241 4B left, data from Fig. 3B) were also observed with DENV, with the CC071 mice displaying the
242 highest plasma viral load after mAb treatment. DENV infection was overall much less clinically
243 severe since only B6-*Ifnar1* mice developed non-lethal symptoms including ruffled fur, hunched
244 back and ataxia.

245 We also investigated the susceptibility of the selected CC strains to WNV. *Oas1b* was
246 previously shown to be a major host genetic determinant of susceptibility to WNV in mice (61).
247 Of note, the three selected CC strains carry the same truncated, non-functional allele of *Oas1b*
248 inherited from the laboratory strain founders (Table 1), conferring them susceptibility to WNV
249 infection. CC mice were infected IP with 10^4 FFUs of WNV IS-98-ST1 and monitored for 14
250 days p.i. (efficient WNV infection does not require anti-IFNAR mAb treatment in *Oas1b*-
251 truncated mice). All CC071 mice died 7 days p.i., significantly faster than CC001 and CC005
252 mice (logrank, $p < 0.01$; Fig. 4C, left panel), indicating that genetic diversity between CC strains
253 also influences their susceptibility to WNV even in the context of *Oas1b* deficiency.

254 To assess whether the differences of susceptibility between these CC strains also applied to
255 other viruses, we infected them with 10^2 PFUs of RVFV ZH548 IP. No significant difference
256 was found between the three CC strains (logrank, $p > 0.3$ for all pairwise comparisons; Fig. 4C,
257 right panel) which succumbed late from the infection, like the commonly used BALB/cByJ mice.
258 Only CC001 mice died significantly later than BALB/c mice (logrank, $p = 0.04$).

259 **Genetic analysis suggests a polygenic control of susceptibility to ZIKV in CC mice**

260 To identify host genetic factors controlling the susceptibility to ZIKV in CC strains, we
261 performed a genome-wide association study between the plasma viral loads at days 2 and 6 p.i.
262 or the decrease rate of plasma viral load, and the genotypes of the 35 CC strains. Genetic
263 associations were plotted as LOD scores. We did not find any genome locations at which LOD

264 scores reached the minimum 0.1 significance threshold for any of the three traits (Fig. 5), which
265 would be expected if phenotypic variations were controlled by one or two loci with strong
266 effects. Therefore, these results suggest that plasma viral load is controlled by multiple small-
267 effect genetic variants.

268 **Genetic diversity of CC strains controls brain viral load and pathology**

269 To assess the influence of host genetics on the brain pathology caused by ZIKV infection,
270 we further characterized the three previously selected CC strains. We measured the viral load in
271 the brain 6 days after IP infection with FG15 ZIKV in mAb-treated CC mice and 129-*Ifnar1*
272 mice (Fig. 6A). CC005 and CC071 which had higher peak plasma viral load also had higher
273 brain viral load (mean=6.5 log₁₀ copies/μg RNA for CC005 and CC071, compared with 5 log₁₀
274 copies/μg RNA for CC001). As expected, 129-*Ifnar1* mice showed the highest viral load in the
275 brain. These results indicate overall correlation between plasma and brain viral loads.

276 Histopathological analysis, carried out in the brain of the same mice (Fig. 6B-N), revealed
277 different lesion profiles between the four mouse strains (Fig. 6B, F, I and L for low
278 magnification images). 129-*Ifnar1* mice clearly displayed the most severe inflammatory lesions
279 with subacute leptomeningo-encephalitis (*i.e.* infiltration of perivascular spaces and
280 leptomeninges by lymphocytes, plasma cells and macrophages; Fig. 6B-E) and activation of
281 microglial cells with microglial nodules (Fig. 7B-D). By contrast, almost no histological lesions
282 were detected in the brain of CC001 mice (Fig. 6F-H), with normal, non-activated, microglial
283 cells (Fig. 7E-G). Only very rare small clusters of activated microglial cells were detected.
284 CC005 displayed moderate inflammatory lesions characterized by perivascular cuffing (Fig. 6I-
285 K), activation of microglial cells (hyperplasia and thickening of cell processes) and microglial
286 nodules (Fig. 7H-J). CC071 mice displayed almost no lesions in HE (Fig. 6L-N) but
287 inflammatory lesions of intermediate severity with activation of microglial cells and microglial

288 nodules (Fig. 7K-M) similar to that of 129-*Ifnar1* mice (Fig. 7A), as revealed by Iba1
289 immunolabeling.

290 The nature and intensity of brain histological lesions may depend on the circulating viral
291 load, on the capacity of the virus and of the mAb to cross the blood-brain barrier and on the
292 permissiveness of brain cells (in particular neurons and microglia). To assess the differences in
293 susceptibility of brain cells between CC strains, we performed intra-cerebral infections to deliver
294 the virus directly into the brain tissue. 129-*Ifnar1* and mAb-untreated CC mice received 10^5
295 FFUs of FG15 ZIKV in the left ventricular region of the brain and were followed for 3 weeks.
296 Mild and transient symptoms (ruffled fur, hunched back) were observed in a few mice of the
297 three strains and one CC005 mouse died on day 19 p.i. A second group of CC mice were infected
298 similarly and euthanized at day 6 p.i. for histological analysis. Differences in brain viral load
299 between CC strains were similar to those observed after IP infection, with CC005 and CC071
300 mice showing significantly higher brain viral load than CC001 mice (Fig. 8A). Compared with
301 IP route of infection, lesions in 129-*Ifnar1* mice were mostly similar, with marked subacute
302 leptomeningo-encephalitis (Fig. 8B-E) and activation of microglial cells (Fig. 9B-D). By
303 contrast, lesion profiles were clearly different in the three CC strains. Two of the five CC001
304 mice displayed no significant histological lesions with normal resting microglial cells, while the
305 other three displayed minimal lesions with gliosis (Fig. 8F-H), and rare small clusters of
306 activated microglial cells (Fig. 9E-G). By this route of infection, CC005 mice displayed
307 heterogeneous lesion profiles with either suspected meningitis and gliosis (Fig. 8I-K, 4/5 mice)
308 or moderate leptomeningo-encephalitis (1/5 mice). Activation of microglial cells with variable
309 severity was detected in all animals (Fig. 9H-J). Strikingly, all CC071 mice displayed marked
310 leptomeningo-encephalitis (Fig. 8L-O) with the strongest activation of microglial cells (Fig. 9K-
311 M and Fig. 9A).

312 These results indicate that CC strains differ in their permissiveness to viral replication in the
313 brain and in their susceptibility to ZIKV-induced histological brain damage. The comparison
314 between IP and IC infection routes shows that these variations cannot be explained only by the
315 possibility of differential dissemination of ZIKV from the circulation to the brain between CC
316 strains.

317 **Viral replication in CC071 cells is increased *in vitro***

318 Differences in peak plasma viral load and the results from IC infections suggested that
319 different efficiencies of viral replication could contribute to the variations in susceptibility
320 between CC strains. To address this point, we measured the production of infectious viral
321 particles in MEFs derived from the CC001 and CC071 strains. Cells were infected with ZIKV
322 FG15 at a MOI of 5. While viral titers remained stable in CC001 between 24 and 72 hours, the
323 production of viral infectious particles by CC071 MEFs increased very significantly over the
324 same period (Fig. 10). These results suggest that increased replication efficiency in CC071 mice
325 could contribute to their susceptible phenotype.

326

327 **DISCUSSION**

328 ZIKV is a serious public health concern considering the occurrence of severe neurological
329 complications in adults and congenital malformations that can result from the infection of
330 pregnant women. The variable outcomes of ZIKV infection in humans has led investigators to
331 hypothesize a role for host genetic factors (9, 13) although this has never been demonstrated thus
332 far. As for other infectious diseases, human genetic studies on susceptibility to ZIKV would
333 require large cohorts of patients and would be confounded by pathogen genetics, pathogen dose,
334 mosquito-dependent factors and multiple environmental parameters. Also, due to the randomness
335 of virus infections, trios are not available for genetic analyses.

336 Several mouse models of human ZIKV infection have already been described and have
337 substantially improved our understanding of viral tropism, dissemination, pathogenesis,
338 persistence, transmission and vaccine protection. To overcome the inability of ZIKV to inhibit
339 IFN induction and signaling pathways in mice as was observed in humans (27), most studies
340 have been performed using *Ifnar1*-deficient mice which have become a reference model.
341 However, high levels of viral replication can also be achieved by temporary inhibition of IFN
342 signaling by anti-IFNAR mAb treatment (30, 31, 62) or even in immunocompetent mice by
343 infecting neonates (36, 63-65) or using a combination of mouse-adapted ZIKV strains and
344 human STAT2 knock-in mice (66).

345 The choice of the ZIKV strain used in an animal model is important to maximize the
346 relevance of mouse studies to human infection. Previous mouse studies have used different
347 ZIKV strains from the African or Asian lineages. Mouse-adapted strains of the African lineage
348 derived from a large number of serial passages are more pathogenic in mice at lower doses (34)
349 but carry mutations that may bias the translatability of results to humans. To avoid this
350 limitation, mouse studies have often used different ZIKV strains from the Asian lineage derived

351 from clinical isolates. Genetic differences between these two lineages are suspected to be
352 responsible for the emergence of symptomatic cases in human starting with the Yap Island
353 epidemics in 2007 (7, 8). Therefore, while the ZIKV strain needs to be standardized in
354 experimental studies, generalization of the results obtained with one viral strain require
355 confirmation using another strain. Because of the incidence of neurological complications
356 associated with infections by Asian lineage ZIKV, we used for our genetic screening a low-
357 passage strain derived from a 2015 case of French Guyana, at an early stage of the South-
358 American epidemics. Since this strain had not been adapted to the mouse, high doses were
359 required to achieve high circulating viral loads.

360 Most mouse studies have used either B6-*Ifnar1* or 129-*Ifnar1* strains without specific
361 rationale and their results cannot be directly compared due to many experimental differences
362 such as ZIKV strain, dose and route of inoculation (67). Under strictly identical conditions, we
363 found that B6-*Ifnar1* mice developed more rapid and severe clinical symptoms and higher
364 mortality than 129-*Ifnar1* mice, despite similar levels of plasma viral RNA at day 2 p.i. We also
365 found that viral load persisted longer in B6-*Ifnar1* mice. These results show that, under our
366 experimental conditions, these two *Ifnar1*-deficient strains have clearly distinct susceptibility to
367 ZIKV. To our knowledge, these two strains have been compared in only one study which found
368 no difference in survival after WNV infection (68). However, their extreme susceptibility might
369 have prevented the identification of any difference. Our results have practical implications for
370 many studies based on *Ifnar1*-deficient mice and motivate further genetic studies to identify the
371 determinants and mechanisms controlling differences of susceptibility between B6 and 129
372 inbred backgrounds.

373 To further investigate the role of host natural genetic variants on ZIKV susceptibility, we
374 leveraged the genetic diversity across CC strains. The CC has been developed as a collection of

375 inbred strains that more accurately reproduce the genetic diversity and phenotypic range seen in
376 human population (69). To enable systemic ZIKV replication after parenteral inoculation in
377 diverse genetic backgrounds, we blocked type I IFN response using MAR1-5A3 mAb (23, 31).

378 Several lines of evidence demonstrate that the mAb treatment was effective in all CC strains.
379 First, we showed similar abrogation of IFN α -induced STAT1 phosphorylation in MEFs from B6
380 and two CC strains carrying the most divergent *Ifnar1* haplotypes (Fig. 2A). Moreover, the
381 differences in peak plasma viral load across 35 CC strains were not associated with the *Ifnar1*
382 allele each CC has received from the founder strains. Secondly, the peak viral load in all mAb-
383 treated CC mice was at least 2.5 logs higher than that of untreated CC071 mice (Fig. 2B and 3B).
384 Finally, we showed, in two CC strains, that increasing the dose of mAb to 4 mg did not modify
385 plasma viral loads at days 2 and 6 p.i. (Fig. 2F), indicating that the 2 mg dose was not limiting.
386 This is consistent with the 5.2 days half-life of the MAR1-5A3 antibody previously reported
387 (30). These results validate that the MAR1-5A3 mAb is effective across a broad range of mouse
388 genetic backgrounds, which will be useful to develop new models of viral infections.

389 A single injection of MAR1-5A3 mAb 24 hours before ZIKV infection resulted in moderate
390 to very high levels of viral RNA in the blood and brain. ZIKV infection was symptomatic in a
391 minority of CC strains (3/35), as observed in infected humans (9, 70), and mortality was
392 observed only in CC071. These results confirm that ZIKV can replicate and establish viremia
393 without inducing symptoms (29). Moreover, while all symptomatic strains had high peak viral
394 loads, other strains with similar viral loads (like CC005 or CC061) never developed any signs of
395 acute illness, indicating that other pathogenic mechanisms are required to result in symptomatic
396 infection and that viral load alone does not reliably predict clinical outcome of ZIKV infection in
397 a genetically diverse mouse population.

398 Since all experimental parameters were carefully standardized between strains (in particular,
399 the microbiological environment in which they were bred), which resulted in small intra-strain
400 variations, and since the MAR1-5A3 mAb treatment was effective across all CC strains,
401 differences in peak viral load between strains can be confidently attributed to host genetic
402 variants. The 86% broad sense heritability further indicates that genetic background is the
403 principal factor driving peak viral load across CC strains.

404 Viremia decreased between days 2 and 6 p.i., as previously reported in several studies (55,
405 71, 72) but not in others (29, 56) for reasons that have not been discussed and remain unclear. In
406 our study, the rate of decrease, which was estimated as the difference of the \log_{10} plasma viral
407 load between day 2 and day 6 p.i., showed remarkable homogeneity between individuals of the
408 same CC strain and very large variations across CC strains. Injecting additional doses of mAb
409 during the course of infection did not modify the kinetics of viral load (Fig. 2F), ruling out the
410 potential role of differential rates of antibody turnover. These results demonstrate a strong
411 influence of host genes on the clearance rate of ZIKV from the blood stream. The decrease of
412 circulating viral load is the net result of ZIKV production in infected tissues, dissemination to the
413 blood stream and elimination from the circulation. Therefore, host genes could control the
414 kinetics of viral load through multiple mechanisms.

415 After exploring the range of susceptibility to ZIKV across broad genetic diversity, we
416 focused our study on a few CC strains exhibiting contrasted phenotypes with the aim of
417 characterizing new models (54). CC001 is one of the least permissive to ZIKV, with low peak
418 viral load. At the other extreme of the distribution, CC005 and CC071 have similarly high
419 plasma viral loads while only CC071 shows symptoms and high mortality. These differences
420 between CC strains were strikingly conserved with the African, mouse-adapted, HD78788 strain
421 (Fig. 4A). The use of lower infectious doses with HD78788 virus was supported by its higher

422 pathogenicity resulting from mouse adaptation. The consistency between these two experiments
423 suggest that the large phenotypic diversity we have reported should apply to most ZIKV strains.

424 Overall, brain viral load and brain pathology after IP infection were consistent with peak
425 plasma viral load. In CC mice, the most notable microscopic lesions included signs of
426 neuroinflammation evidenced by Iba1 immunohistochemistry. Neuroinflammation was similar in
427 129-*Ifnar1*, CC005 and CC071 mice. These changes were less pronounced than in a previous
428 study which reported more severe CNS lesions in MAR1-5A3-treated B6 mice (31), infected
429 with a more virulent African lineage ZIKV strain. The variable severity of lesions observed in
430 CC mice, ranging from very mild abnormalities in CC001, to inflammatory lesions with
431 perivascular cuffing, activation of microglial cells and microglial nodules in CC005, indicates
432 that the genetic background also controls ZIKV neuropathogenesis.

433 The less severe histological lesions observed in CC mice compared with 129-*Ifnar1* mice
434 could be due to the limited access to the brain of the virus or of the mAb which does not
435 appreciably cross the blood-brain barrier (29). Therefore, intracerebral infection aimed at
436 comparing brain lesions between strains while controlling the amount of virus effectively
437 delivered. Surprisingly, CC001 and CC005 mice showed similar types and severity of lesions
438 (although not all CC001 mice showed lesions) while CC071 mice developed much more severe
439 signs of leptomeningo-encephalitis with massive neuroinflammation, similar to those of 129-
440 *Ifnar1* mice. This last result suggests that the milder lesions observed in CC071 compared with
441 129-*Ifnar1* mice after IP infection were likely due to reduced viral dissemination to the brain.
442 Importantly, mice did not receive prior mAb treatment, allowing for the development of local
443 and systemic antiviral responses. These results emphasize the complex interplay between
444 infected cells and effectors of the immune response, which likely differs between CC strains
445 under the control of host genes.

446 Viral replication rate between resistant CC001 and highly susceptible CC071 mice was
447 investigated as a plausible mechanism for the differences in susceptibility between these two
448 strains. MEFs are a semi-permanent source of cells which have been extensively used to assess
449 viral replication (73, 74) including with ZIKV (75, 76). In CC001 MEFs, the production of
450 infectious viral particles was stable between 24 and 48h and decreased between 48 and 72h,
451 while it steadily increased over time in CC071 MEFs, leading to significantly higher viral titers
452 starting at 48h. Our data is consistent with the observation by Caires-Junior et al. who reported
453 increased ZIKV replication rate in iPS-derived neuroprogenitor cells from CZS-affected babies
454 compared with their unaffected dizygotic twin (13). Therefore, our results strongly suggest that
455 increased replication rate in CC071 compared with CC001 likely contributes to its higher plasma
456 and brain viral loads and to its higher overall susceptibility to ZIKV.

457 Investigating the genetic diversity of a large number of CC strains has significantly extended
458 the range of phenotypes induced by ZIKV infection in mice and better model the heterogeneity
459 of the human population. It has allowed testing important factors such as mouse gender and the
460 method of viral load measurement across multiple host genetic background, providing robust
461 conclusions (37). Importantly, we found no differences between male and female mice in their
462 susceptibility to ZIKV disease, nor in the peak viral load (Fig. 2E). We also found a high
463 correlation between viral loads measured by titration and by qRT-PCR over a 2 log₁₀ range (Fig.
464 2D). This is in contrast with a study on Ebola virus which showed that, in spleen and liver, the
465 susceptible mice produced similar amounts of viral genomes but 1 to 2 log₁₀ more infectious
466 virions than the resistant mice (43).

467 Genetic diversity also allowed us to assess correlations between traits, which cannot be
468 achieved in a single strain. We showed that brain viral load at day 6 after IP was consistent with
469 plasma viral load at day 2 p.i., but that plasma viral loads at days 2 and 6 p.i. were only

470 moderately correlated. Likewise, we found that clinical severity did not correlate with the
471 intensity of brain histological lesions and neuroinflammation, as summarized in Table 3. These
472 dissociations between phenotypes provide evidence for partly distinct mechanisms and genetic
473 control (37) and lead to distinct mouse models.

474 A recent study has reported strain-dependent variations in the long-term neuropathological
475 and behavioral consequences of ZIKV infection after neonatal infection between four mouse
476 inbred strains known to differ in their susceptibility to pathogens (36). Since they are all
477 laboratory strains, they do not cover the same genetic variation as in our study and it is likely that
478 even more diverse phenotypes would be observed in this model with the CC panel.

479 Genetic analysis of our results strongly suggests that, by contrast with other viruses for
480 which major host genetic determinants have been identified (e.g. *Oas1b* for WNV (61) or *Mx1*
481 for influenza virus (77)), susceptibility to ZIKV in CC strains is under polygenic control. This is
482 supported by the continuous distributions, across the CC strains, of the values of peak plasma
483 viral load (Fig. 3B) and of the rate of viral decrease (Fig. 3C), and by the absence of any regions
484 of the genome significantly associated with variations in viral load (Fig. 5). Calculations based
485 on CC genotypes show that, with 35 strains and an average of 5 mice per strain, we had 80%
486 power of detecting a bi-allelic QTL explaining 30% or more of the phenotypic variance (78).
487 This clearly rules out the possibility that the phenotypic variations measured across CC strains
488 were controlled by one or few genes with major effects, as observed with *Oas1b* for WNV (47).
489 Dissecting the genetic architecture of resistance and susceptibility to ZIKV in these strains will
490 require combining complementary strategies. Intercrosses between contrasted strains such as
491 CC001 and CC071 will reduce genetic complexity and may result in increased power for QTL
492 mapping due to larger sample size (54). However, the mapping resolution achieved in an F2 or a
493 backcross leads to large genetic intervals. Other approaches, such as gene expression studies on

494 various cell types (such as immune cells, neurons or glial cells) will be used to identify
495 differentially activated host response pathways and reduce the number of candidate genes in
496 these intervals.

497 *Oas1b* is an interferon-stimulated gene and a major determinant of mouse susceptibility to
498 WNV (45). A variant in OAS3, a member of the human homologous gene family, has been
499 associated with increased severity of dengue (79). Most laboratory strains, including five of the
500 eight CC founders, carry the same non-functional allele of *Oas1b* which renders them susceptible
501 to WNV infection (61), while the three wild-derived CC founders carry polymorphic but
502 functional alleles and are resistant (45). CC strains therefore carry either functional or non-
503 functional *Oas1b* alleles. Our results provide multiple lines of evidence to rule out a significant
504 role of *Oas1b* in the variations of susceptibility to ZIKV across CC strains. First, since mAb-
505 mediated blockade of type I IFN response likely inhibits temporarily *Oas1b* induction, *Oas1b*
506 allele is unlikely to explain differences in peak viral load at day 2 p.i. Moreover, our QTL
507 mapping analysis showed that mouse genotype at *Oas1b* (located on distal chromosome 5) did
508 not significantly contribute to variations in viral load at day 2 or day 6 p.i., or in the rate of viral
509 load decrease (Fig. 5). Finally, since both CC001, CC005 and CC071 strains carry the *Oas1b*
510 truncated allele (Table 1), their differences in clinical severity, brain pathology and replication
511 rate in infected cells must be controlled by other genetic variants. Interestingly, the large
512 difference of survival time after WNV infection between CC071 and CC001 or CC005 provides
513 ideal strain combinations to identify novel genes controlling susceptibility to this virus.

514 Out of this large series of CC strains, we identified several new mouse models of ZIKV
515 disease. CC071 mice were the most susceptible to ZIKV infection, more than mAb-treated B6
516 mice (Fig. 3A,B). mAb treatment was required to achieve high circulating viral load (Fig. 2B),
517 showing that CC071 has functional type I IFN response. CC071 mice were also very susceptible

518 to DENV and WNV, two flaviviruses related to ZIKV. However, they are not uniformly
519 susceptible to infectious agents since they showed susceptibility to RVFV similar to that of
520 BALB/c, CC001 and CC005 mice, and intermediate susceptibility to *Salmonella* Typhimurium
521 (52). Together with other susceptible strains like CC021 and CC026 which developed symptoms,
522 or CC005 which developed severe brain lesions, CC071 will help identifying mechanisms of
523 severe ZIKV infection and their genetic control. By contrast, CC001 mice were highly resistant,
524 even to a strongly pathogenic African ZIKV strain, despite blockade of type I IFN signaling.
525 Extensive analysis of these CC strains with extreme phenotypes may elucidate how genetic
526 variants affect susceptibility as well as innate and adaptive immune responses to flaviviral
527 infection (54) and provide deeper understanding of the pathophysiology of severe complications
528 of human ZIKV disease.

529

530 **MATERIALS AND METHODS**

531

532 **Mice**

533 All Collaborative Cross (CC) mice (purchased from the Systems Genetics Core Facility,
534 University of North Carolina and bred at the Institut Pasteur) (80), C57BL/6J mice (purchased
535 from Charles River Laboratories France), BALB/cByJ and *Ifnar1* knock-out mice (*Ifnar1*^{tm1Agt}
536 allele on 129S2/SvPas or C57BL/6J background, designated 129-*Ifnar1* and B6-*Ifnar1*,
537 respectively, and bred at the Institut Pasteur) were maintained under SPF conditions with 14:10
538 light-dark cycle and *ad libitum* food and water in the Institut Pasteur animal facility. All CC
539 strains bred at the Institut Pasteur were included in this study. In all experiments, mice were
540 killed by cervical dislocation. All experimental protocols were approved by the Institut Pasteur
541 Ethics Committee (projects #2013-0071, #2014-0070, #2016-0013, #2016-0018 and dap190107)
542 and authorized by the French Ministry of Research (decisions #00762.02, #7822, #6463, #6466
543 and #19469, respectively), in compliance with French and European regulations.

544

545 **Cell lines**

546 Vero cells (ATCC CRL-1586) were cultured at 37°C in Dulbecco's Modified Eagle Medium
547 (DMEM, Gibco) supplemented with 10% fetal bovine serum (FBS, Eurobio). C6/36 cells
548 (ATCC CRL-1660) were cultured at 28°C in Leibovitz Medium (L-15 Medium, Gibco)
549 supplemented with 10% FBS, 1% Non-Essential Amino Acids (Life Technologies) and 1%
550 Tryptose Phosphate Broth (Life Technologies).

551

552 **Viruses**

553 The FG15 Asian Zika virus (ZIKV) strain, isolated from a patient during ZIKV outbreak in
554 French Guiana in December 2015, was obtained from the Virology Laboratory of the Institut
555 Pasteur of French Guiana. The HD78788 African ZIKV strain, isolated from a human case in
556 Senegal in 1991, was obtained from the Institut Pasteur collection. The KDH0026A DENV
557 serotype 1 (DENV-1) strain, isolated from a patient in Thailand in 2010, was previously
558 described (81). Viral stocks were prepared from supernatant of infected C6/36 cells, clarified by
559 centrifugation at 800g and titrated on Vero cells by focus-forming assay (FFA). Stocks were kept
560 at -80°C. The West Nile virus (WNV) strain IS-98-ST1 (or Stork/98) was obtained, cultured and
561 used as described in Mashimo *et al.* (61). The Rift Valley Fever virus (RVFV) strain ZH548 was
562 obtained, cultured and used as described in Tokuda *et al.* (82).

563

564 **Mouse experiments**

565 All infection experiments were performed in a biosafety level 3 animal facility. Mice were
566 maintained in isolators.

567 ZIKV and DENV systemic infection. CC mice received 2 mg of IFNAR-blocking mouse
568 mAb (MAR1-5A3, BioXCell) by intraperitoneal (IP) injection one day before ZIKV or DENV
569 infection (83). Groups of 6-8 week-old mice were inoculated IP with 10^7 focus-forming units
570 (FFUs) of ZIKV FG15 or 10^3 FFUs of ZIKV HD78788, in 200 μ L PBS. For DENV infection,
571 mice were anesthetized by IP injection with a solution of Xylazine (5 mg/kg) and Ketamine (80
572 mg/kg) and afterwards inoculated by intravenous (IV) injection in the retro-orbital sinus with
573 2.10^6 FFUs of DENV-1 KDH0026A, in 100 μ L PBS. Survival and clinical signs were monitored
574 daily for up to 14 days. Clinical signs were scored as follows: 0, no symptom; 1, ruffled fur; 2,
575 emaciation, hunched posture and/or hypo activity; 3, hind limb weakness, prostration and/or

576 closed eyes; 4, moribund or dead. Blood samples were collected at several time points from the
577 retromandibular vein for plasma viral load assessment.

578 ZIKV intracerebral infection. Mice were anesthetized by IP injection with a solution of
579 Xylazine (5 mg/kg), Ketamine (75 mg/kg) and Buprenorphine (0.03 mg/kg). Groups of 5-6
580 week-old mice were then inoculated by intracerebral (IC) injection in the right brain hemisphere
581 with a 26-gauge needle affixed to a Hamilton syringe sheathed by a wire guard allowing no more
582 than a 4-mm penetrance into the skull cavity, as described in (84). Mice received either 10^5 FFUs
583 of ZIKV FG15 in PBS or PBS alone, in a volume of 10 μ L. Survival and clinical signs were
584 monitored daily for 6 days and euthanized for brain collection. Another cohort of mice (n=7-8
585 per strain) was infected similarly and monitored daily for 21 days to assess symptoms and
586 survival.

587 WNV and RVFV infection. Groups of 8-12 week-old mice were inoculated IP with 10^3
588 FFUs of WNV strain IS-98-ST1 or 10^2 PFUs of RVFV strain ZH548. Survival and clinical signs
589 were monitored daily for up to 14 days (RVFV) or 21 days (WNV).

590

591 **Mouse embryonic fibroblasts (MEFs) isolation and infection**

592 MEFs were isolated from individual fetuses from one or more genetically identical females
593 at day 13.5-14.5 of gestation, and cultured in DMEM supplemented with 10% FBS (Eurobio)
594 and 1% penicillin/streptomycin (Gibco) at 37°C. MEFs were used until passage 2.

595 MEFs were plated at identical densities in culture dishes 24 hours before infection. MEFs
596 were infected with ZIKV FG15 strain at a MOI of 5. After 2 hours of incubation at 37°C, the
597 inoculum was replaced with fresh medium. Supernatants were collected at 24, 48 and 72 hours
598 post-infection. Titration was performed by FFA in Vero cells.

599

600 **Focus-forming assay**

601 Vero cells were seeded at $3 \cdot 10^4$ per well in 100 μ l complete medium (DMEM, FBS 10%) in
602 96-well plates. After overnight incubation at 37°C, medium was replaced with 40 μ L of serial
603 10-fold dilutions of the samples, and 115 μ L of methylcellulose overlay was added 2 hours later.
604 After 40 hours incubation, culture medium was removed and cells were fixed with 100 μ L/well
605 of 4% paraformaldehyde for 20 minutes and permeabilized with a solution of 0.3% Triton and
606 5% FBS in PBS for 20 minutes. Cells were washed, incubated with a mouse mAb directed
607 against ZIKV envelop protein (4G2, purified from the ATCC hybridoma) for 1 hour at 37°C
608 (1/250° in blocking buffer). Cells were further washed, incubated with secondary antibody
609 (AlexaFluor-488-conjugated anti-mouse IgG, Invitrogen) for 45 minutes at 37°C and washed.
610 Infected cell foci were counted using an ImmunoSpot CTL analyzer and viral titers were
611 calculated from the average number of foci.

612

613 **Viral genome quantification by RT-qPCR**

614 Blood samples were centrifuged to recover plasma from which viral RNA was extracted
615 with the QIAamp Viral RNA Mini Kit (Qiagen). Brain samples were homogenized at 4°C in 1
616 mL of TRIzol reagent (Life Technologies) using ceramic beads and automated homogenizer
617 (PreCellys). Total RNA was extracted according to manufacturer's instructions. cDNA synthesis
618 was performed using MMLV reverse transcriptase (Life Technologies) in a Bio-Rad *Mycycler*
619 thermocycler. ZIKV and DENV cDNA were quantified by TaqMan quantitative PCR (qPCR) in
620 a ViiA7 Instrument (Life Technologies) using standard cycling conditions. Primer sets adapted
621 from previous works (85-87) were used to detect ZIKV and DENV RNA. ZIKV FG15: forward,
622 5'-CCG CTG CCC AAC ACA AG- 3'; reverse, 5'-CCA CTA ACG TTC TTT TGC AGA CAT-
623 3'; probe, 5'-6FAM-AGC CTA CCT TGA CAA GCA ATC AGA CAC TCA A-MGB- 3' (Life

624 Technologies). ZIKV HD78788: forward, 5'-AAA TAC ACA TAC CAA AAC AAA GTG GT-
625 3'; reverse, 5' -TCC ACT CCC TCT CTG GTC TTG- 3'; probe, 5'-6FAM-CTC AGA CCA
626 GCT GAA G-MGB- 3' (Life Technologies). DENV-1 KDH0026A: forward, 5' –GGA AGG
627 AGA AGG ACT CCA CA- 3'; reverse, 5' - ATC CTT GTA TCC CAT CCG GCT- 3'; probe, 5'
628 -6FAM CTC AGA GAC ATA TCA AAG ATT CCA GGG-MGB- 3' (Life Technologies). Viral
629 load is expressed on a Log₁₀ scale as viral genome copies per milliliter (plasma samples) or per
630 total RNA microgram (brain samples) after comparison with a standard curve produced using
631 serial 10-fold dilutions of a plasmid containing the corresponding fragment of ZIKV genome.

632

633 **Western Blot analysis**

634 MEFs ($5 \cdot 10^6$) were pre-incubated with 100 µg IFNAR1-blocking antibody (MAR1-5A3,
635 BioXCell) for 7 hours and then stimulated, or not, with 300 IU/mL mouse IFN- α (Miltenyi
636 Biotec) for 15 minutes. MEFs were detached and centrifuged at 300xg for 5 minutes and cell
637 pellet was re-suspended in cold PBS. MEFs were then lysed into extraction buffer (10 mM Tris–
638 HCl, pH 7.5, 5 mM EDTA, 150 mM NaCl, 1% NP40, 10% glycerol, 30 mM NaP, 50 mM
639 NaFluoride) completed with protease inhibitor (Complete, EDTA free, Roche) and phosphatase
640 inhibitors (phosStop easy pack, Roche) with 2.5 UI of benzonase nuclease (Sigma). Lysates were
641 incubated on ice for 30 minutes and non-soluble fraction was separated by centrifugation. Protein
642 concentrations were determined by Bradford assay, and equal amounts of protein were further
643 used. Protein denaturation was performed in Laemmli buffer at 95°C for 5 minutes. After
644 separation on a 12% polyacrylamide gel (Biorad), proteins were transferred on Immun-Blot
645 polyvinylidene difluoride (PVDF) membrane (Biorad) and incubated overnight with the
646 following antibodies: Anti-Phospho-Stat1 Tyr701 (1/1,000^e, #9167, Cell Signaling), Anti-Total
647 Stat1 N-terminus (1/500^e, # 610115, BD Biosciences), Anti- α Tubulin (1/8,000^e, # T5168,

648 Merck). Membranes were incubated for 1.5 hour at room temperature with an anti-mouse or an
649 anti-rabbit IgG horseradish peroxidase-linked secondary antibody (1/10,000^e, NA931 and
650 NA934V, Amersham) and signals were visualized using autoradiography.

651

652 **Histopathology**

653 After necropsy, brain was removed, fixed for 48-72 hours in 10% neutral-buffered formalin
654 and embedded in paraffin; 4µm-thick sections were stained in hematoxylin-eosin. Morphology
655 of microglial cells was assessed by immunohistochemistry using rabbit anti-Iba1 primary
656 antibody (# 01919741, Wako chemical, dilution 1:50) as previously described (88). Sections
657 were analyzed by a trained veterinary pathologist in a blind study on coded slides. Quantification
658 of the microglia reaction was carried out using automated detection of the Iba1 labeling signal
659 and measurement of the labelled area on a low magnification (x2) picture of a brain section of
660 each mouse, using ImageJ software (<https://imagej.nih.gov/ij/>).

661

662 **Genetic analysis**

663 Broad sense heritability was calculated as previously described (60).

664 Plasma viral load at days 2 and 6 p.i. and plasma viral load decrease, measured on 159 mice
665 from 35 CC strains (average of 4.5 mice per strain), were used in quantitative trait locus (QTL)
666 mapping using the *rqt12* R package (89) and GigaMUGA genotypes of CC founders and CC
667 strains available from <http://csbio.unc.edu/CCstatus/CCGenomes/#genotypes>. Genome scan was
668 performed using the *scan1* function with a linear mixed model using a kinship matrix. Statistical
669 significance levels were calculated from 1,000 permutations.

670 Genotype-phenotype associations for specific genes (*Ifnar1*, *Oas1b*) were tested by Kruskal-
671 Wallis test using the founder haplotype as the genotype.

672

673 **Statistical analysis**

674 Statistical analyses were performed using R software (v3.5.2). Kaplan-Meier survival curves
675 were compared by logrank test. Two-way ANOVA was used for testing mouse strain and sex
676 effects on plasma viral load at day 2 p.i. (Fig. 2E). Student's *t*-test was used to compare viral
677 loads in tissues, except when data showed heterogeneous variance between groups, in which case
678 we used Kruskal-Wallis and Wilcoxon non-parametric tests. These tests were also used for
679 assessing mouse strain effect on plasma viral load and on plasma viral load decrease (Fig. 3).
680 Pearson's coefficient was used for the correlation between plasma viral load at days 2 and 6 p.i.
681 (Fig. 3B) and for the correlation between measurements of plasma viral load by FFA and RT-
682 qPCR (Fig. 2D). Student's *t*-test was used to compare viral titers between strains in *in vitro*
683 experiments. P-values < 0.05 were considered statistically significant.

684

685

686 **NOTES**

687 We are grateful to the Virology Laboratory of the Institut Pasteur of French Guyana
688 (National Reference Center for Arboviruses) for providing the FG15 ZIKV strain and Valérie
689 Choumet for providing the IS-98-ST1 WNV strain. We thank Thérèse Couderc and Claude
690 Ruffié for providing B6-*Ifnar1* and 129-*Ifnar1* mice, Laetitia Joullié and Marion Doladilhe for
691 technical help, Magali Tichit for histopathology techniques, Isabelle Lanctin, Tommy Penel and
692 Jérôme Le Boydre for careful breeding of CC mice, and the animal facility staff for animal care
693 in biocontainment units (DTPS-C2RA-Central Animal Facility platform). We are grateful to Jean
694 Jaubert, Michel Cohen-Tannoudji and Aurore Vidy-Roche for useful discussions throughout the
695 project, and to Rachel Meade for editorial suggestions.

696 The authors declare no competing interests.

697 This work was supported by a grant from the French Government's Investissement d'Avenir
698 program, Laboratoire d'Excellence "Integrative Biology of Emerging Infectious Diseases" (grant
699 n°ANR-10-LABX-62-IBEID). C.M. was supported by a fellowship from the grant n°ANR-10-
700 LABX-62-IBEID.

701

702 **REFERENCES**

- 703 1. **Petersen LR, Jamieson DJ, Powers AM, Honein MA.** 2016. Zika Virus. *N Engl J Med*
704 **374**:1552-1563.
- 705 2. **Talero-Gutierrez C, Rivera-Molina A, Perez-Pavajeau C, Ossa-Ospina I, Santos-**
706 **Garcia C, Rojas-Anaya MC, de-la-Torre A.** 2018. Zika virus epidemiology: from
707 Uganda to world pandemic, an update. *Epidemiol Infect*
708 doi:10.1017/s0950268818000419:1-7.
- 709 3. **Cao-Lormeau VM, Blake A, Mons S, Lastere S, Roche C, Vanhomwegen J, Dub T,**
710 **Baudouin L, Teissier A, Larre P, Vial AL, Decam C, Choumet V, Halstead SK,**
711 **Willison HJ, Musset L, Manuguerra JC, Despres P, Fournier E, Mallet HP, Musso**
712 **D, Fontanet A, Neil J, Ghawche F.** 2016. Guillain-Barre Syndrome outbreak associated
713 with Zika virus infection in French Polynesia: a case-control study. *Lancet* **387**:1531-
714 1539.
- 715 4. **Munoz LS, Parra B, Pardo CA.** 2017. Neurological Implications of Zika Virus
716 Infection in Adults. *J Infect Dis* **216**:S897-s905.
- 717 5. **Rasmussen SA, Jamieson DJ, Honein MA, Petersen LR.** 2016. Zika Virus and Birth
718 Defects--Reviewing the Evidence for Causality. *N Engl J Med* **374**:1981-1987.
- 719 6. **Sanz Cortes M, Rivera AM, Yopez M, Guimaraes CV, Diaz Yunes I, Zarutskie A,**
720 **Davila I, Shetty A, Mahadev A, Serrano SM, Castillo N, Lee W, Valentine G, Belfort**
721 **M, Parra G, Mohila C, Aagaard K, Parra M.** 2018. Clinical Assessment and Brain
722 Findings in a Cohort of Mothers, Fetuses and Infants Infected with Zika Virus. *Am J*
723 *Obstet Gynecol* doi:10.1016/j.ajog.2018.01.012.
- 724 7. **Xia H, Luo H, Shan C, Muruato AE, Nunes BT, Medeiros DBA, Zou J, Xie X,**
725 **Giraldo MI, Vasconcelos PFC, Weaver SC, Wang T, Rajsbaum R, Shi PY.** 2018. An

- 726 evolutionary NS1 mutation enhances Zika virus evasion of host interferon induction. *Nat*
727 *Commun* **9**:414.
- 728 8. **Liu Y, Liu J, Du S, Shan C, Nie K, Zhang R, Li XF, Zhang R, Wang T, Qin CF,**
729 **Wang P, Shi PY, Cheng G.** 2017. Evolutionary enhancement of Zika virus infectivity in
730 *Aedes aegypti* mosquitoes. *Nature* **545**:482-486.
- 731 9. **Flamand C, Fritzell C, Matheus S, Dueymes M, Carles G, Favre A, Enfissi A, Adde**
732 **A, Demar M, Kazanji M, Cauchemez S, Rousset D.** 2017. The proportion of
733 asymptomatic infections and spectrum of disease among pregnant women infected by
734 Zika virus: systematic monitoring in French Guiana, 2016. *Euro Surveill* **22**.
- 735 10. **Cauchemez S, Besnard M, Bompard P, Dub T, Guillemette-Artur P, Eyrolle-**
736 **Guignot D, Salje H, Van Kerkhove MD, Abadie V, Garel C, Fontanet A, Mallet HP.**
737 2016. Association between Zika virus and microcephaly in French Polynesia, 2013-15: a
738 retrospective study. *Lancet* **387**:2125-2132.
- 739 11. **Brasil P, Pereira JP, Jr., Moreira ME, Ribeiro Nogueira RM, Damasceno L,**
740 **Wakimoto M, Rabello RS, Valderramos SG, Halai UA, Salles TS, Zin AA, Horovitz**
741 **D, Daltro P, Boechat M, Raja Gabaglia C, Carvalho de Sequeira P, Pilotto JH,**
742 **Medialdea-Carrera R, Cotrim da Cunha D, Abreu de Carvalho LM, Pone M,**
743 **Machado Siqueira A, Calvet GA, Rodrigues Baiao AE, Neves ES, Nassar de**
744 **Carvalho PR, Hasue RH, Marschik PB, Einspieler C, Janzen C, Cherry JD, Bispo**
745 **de Filippis AM, Nielsen-Saines K.** 2016. Zika Virus Infection in Pregnant Women in
746 Rio de Janeiro. *N Engl J Med* **375**:2321-2334.
- 747 12. **McGrath EL, Rossi SL, Gao J, Widen SG, Grant AC, Dunn TJ, Azar SR, Roundy**
748 **CM, Xiong Y, Prusak DJ, Loucas BD, Wood TG, Yu Y, Fernandez-Salas I, Weaver**

- 749 **SC, Vasilakis N, Wu P.** 2017. Differential Responses of Human Fetal Brain Neural Stem
750 Cells to Zika Virus Infection. *Stem Cell Reports* doi:10.1016/j.stemcr.2017.01.008.
- 751 13. **Caires-Junior LC, Goulart E, Melo US, Araujo BSH, Alvizi L, Soares-Schanoski A,**
752 **de Oliveira DF, Kobayashi GS, Griesi-Oliveira K, Musso CM, Amaral MS, daSilva**
753 **LF, Astray RM, Suarez-Patino SF, Ventini DC, Gomes da Silva S, Yamamoto GL,**
754 **Ezquina S, Naslavsky MS, Telles-Silva KA, Weinmann K, van der Linden V, van**
755 **der Linden H, de Oliveira JMR, Arrais NRM, Melo A, Figueiredo T, Santos S,**
756 **Meira JCG, Passos SD, de Almeida RP, Bispo AJB, Cavalheiro EA, Kalil J, Cunha-**
757 **Neto E, Nakaya H, Andreato-Santos R, de Souza Ferreira LC, Verjovski-Almeida S,**
758 **Ho PL, Passos-Bueno MR, Zatz M.** 2018. Discordant congenital Zika syndrome twins
759 show differential in vitro viral susceptibility of neural progenitor cells. *Nat Commun*
760 **9:475.**
- 761 14. **Julander JG, Siddharthan V.** 2017. Small-Animal Models of Zika Virus. *J Infect Dis*
762 **216:S919-s927.**
- 763 15. **Winkler CW, Peterson KE.** 2017. Using immunocompromised mice to identify
764 mechanisms of Zika virus transmission and pathogenesis. *Immunology*
765 doi:10.1111/imm.12883.
- 766 16. **Li H, Saucedo-Cuevas L, Regla-Nava JA, Chai G, Sheets N, Tang W, Terskikh AV,**
767 **Shresta S, Gleeson JG.** 2016. Zika Virus Infects Neural Progenitors in the Adult Mouse
768 Brain and Alters Proliferation. *Cell Stem Cell* doi:10.1016/j.stem.2016.08.005.
- 769 17. **Rosenfeld AB, Doobin DJ, Warren AL, Racaniello VR, Vallee RB.** 2017. Replication
770 of early and recent Zika virus isolates throughout mouse brain development. *Proc Natl*
771 *Acad Sci U S A* doi:10.1073/pnas.1714624114.

- 772 18. **Tang WW, Young MP, Mamidi A, Regla-Nava JA, Kim K, Shrestha S.** 2016. A
773 Mouse Model of Zika Virus Sexual Transmission and Vaginal Viral Replication. *Cell*
774 *Rep* **17**:3091-3098.
- 775 19. **Duggal NK, McDonald EM, Ritter JM, Brault AC.** 2018. Sexual transmission of Zika
776 virus enhances in utero transmission in a mouse model. *Sci Rep* **8**:4510.
- 777 20. **Winkler CW, Woods TA, Rosenke R, Scott DP, Best SM, Peterson KE.** 2017. Sexual
778 and Vertical Transmission of Zika Virus in anti-interferon receptor-treated Rag1-
779 deficient mice. *Sci Rep* **7**:7176.
- 780 21. **Jaeger AS, Murrieta RA, Goren LR, Crooks CM, Moriarty RV, Weiler AM,**
781 **Rybarczyk S, Semler MR, Huffman C, Mejia A, Simmons HA, Fritsch M, Osorio**
782 **JE, Eickhoff JC, O'Connor SL, Ebel GD, Friedrich TC, Aliota MT.** 2019. Zika
783 viruses of African and Asian lineages cause fetal harm in a mouse model of vertical
784 transmission. *PLoS Negl Trop Dis* **13**:e0007343.
- 785 22. **Yockey LJ, Varela L, Rakib T, Khoury-Hanold W, Fink SL, Stutz B, Szigeti-Buck**
786 **K, Van den Pol A, Lindenbach BD, Horvath TL, Iwasaki A.** 2016. Vaginal Exposure
787 to Zika Virus during Pregnancy Leads to Fetal Brain Infection. *Cell* **166**:1247-
788 1256.e1244.
- 789 23. **Miner JJ, Cao B, Govero J, Smith AM, Fernandez E, Cabrera OH, Garber C, Noll**
790 **M, Klein RS, Noguchi KK, Mysorekar IU, Diamond MS.** 2016. Zika Virus Infection
791 during Pregnancy in Mice Causes Placental Damage and Fetal Demise. *Cell* **165**:1081-
792 1091.
- 793 24. **Paul AM, Acharya D, Neupane B, Thompson EA, Gonzalez-Fernandez G, Copeland**
794 **KM, Garrett M, Liu H, Lopez ME, de Cruz M, Flynt A, Liao J, Guo YL, Gonzalez-**
795 **Fernandez F, Vig PJS, Bai F.** 2018. Congenital Zika Virus Infection in

796 Immunocompetent Mice Causes Postnatal Growth Impediment and Neurobehavioral
797 Deficits. *Front Microbiol* **9**:2028.

798 25. **Caine EA, Jagger BW, Diamond MS.** 2018. Animal Models of Zika Virus Infection
799 during Pregnancy. *Viruses* **10**.

800 26. **Wu Y, Liu Q, Zhou J, Xie W, Chen C, Wang Z, Yang H, Cui J.** 2017. Zika virus
801 evades interferon-mediated antiviral response through the co-operation of multiple
802 nonstructural proteins in vitro. *Cell Discov* **3**:17006.

803 27. **Pierson TC, Diamond MS.** 2018. The emergence of Zika virus and its new clinical
804 syndromes. *Nature* **560**:573-581.

805 28. **Grant A, Ponia SS, Tripathi S, Balasubramaniam V, Miorin L, Sourisseau M,**
806 **Schwarz MC, Sanchez-Seco MP, Evans MJ, Best SM, Garcia-Sastre A.** 2016. Zika
807 Virus Targets Human STAT2 to Inhibit Type I Interferon Signaling. *Cell Host Microbe*
808 **19**:882-890.

809 29. **Lazear HM, Govero J, Smith AM, Platt DJ, Fernandez E, Miner JJ, Diamond MS.**
810 2016. A Mouse Model of Zika Virus Pathogenesis. *Cell Host Microbe* **19**:720-730.

811 30. **Sheehan KC, Lai KS, Dunn GP, Bruce AT, Diamond MS, Heutel JD, Dungo-Arthur**
812 **C, Carrero JA, White JM, Hertzog PJ, Schreiber RD.** 2006. Blocking monoclonal
813 antibodies specific for mouse IFN-alpha/beta receptor subunit 1 (IFNAR-1) from mice
814 immunized by in vivo hydrodynamic transfection. *J Interferon Cytokine Res* **26**:804-819.

815 31. **Smith DR, Hollidge B, Daye S, Zeng X, Blancett C, Kuszpit K, Bocan T, Koehler**
816 **JW, Coyne S, Minogue T, Kenny T, Chi X, Yim S, Miller L, Schmaljohn C, Bavari**
817 **S, Golden JW.** 2017. Neuropathogenesis of Zika Virus in a Highly Susceptible
818 Immunocompetent Mouse Model after Antibody Blockade of Type I Interferon. *PLoS*
819 *Negl Trop Dis* **11**:e0005296.

- 820 32. **Kamiyama N, Soma R, Hidano S, Watanabe K, Umekita H, Fukuda C, Noguchi K,**
821 **Gendo Y, Ozaki T, Sonoda A, Sachi N, Runtuwene LR, Miura Y, Matsubara E,**
822 **Tajima S, Takasaki T, Eshita Y, Kobayashi T.** 2017. Ribavirin inhibits Zika virus
823 (ZIKV) replication in vitro and suppresses viremia in ZIKV-infected STAT1-deficient
824 mice. *Antiviral Res* doi:10.1016/j.antiviral.2017.08.007.
- 825 33. **Jagger BW, Miner JJ, Cao B, Arora N, Smith AM, Kovacs A, Mysorekar IU, Coyne**
826 **CB, Diamond MS.** 2017. Gestational Stage and IFN-lambda Signaling Regulate ZIKV
827 Infection In Utero. *Cell Host Microbe* **22**:366-376 e363.
- 828 34. **Tripathi S, Balasubramaniam VR, Brown JA, Mena I, Grant A, Bardina SV,**
829 **Maringer K, Schwarz MC, Maestre AM, Sourisseau M, Albrecht RA, Krammer F,**
830 **Evans MJ, Fernandez-Sesma A, Lim JK, Garcia-Sastre A.** 2017. A novel Zika virus
831 mouse model reveals strain specific differences in virus pathogenesis and host
832 inflammatory immune responses. *PLoS Pathog* **13**:e1006258.
- 833 35. **Manet C, Roth C, Tawfik A, Cantaert T, Sakuntabhai A, Montagutelli X.** 2018. Host
834 genetic control of mosquito-borne Flavivirus infections. *Mamm Genome*
835 doi:10.1007/s00335-018-9775-2.
- 836 36. **Snyder-Keller A, Kramer L, Zink S, Bolivar VJ.** 2019. Mouse strain and sex-
837 dependent differences in long-term behavioral abnormalities and neuropathologies after
838 developmental zika infection. *J Neurosci* doi:10.1523/jneurosci.2666-18.2019.
- 839 37. **Saul MC, Philip VM, Reinholdt LG, Chesler EJ.** 2019. High-Diversity Mouse
840 Populations for Complex Traits. *Trends in Genetics* doi:10.1016/j.tig.2019.04.003.
- 841 38. **Montagutelli X.** 2000. Effect of the genetic background on the phenotype of mouse
842 mutations. *J Am Soc Nephrol* **11 Suppl 16**:S101-105.
- 843 39. **Nadeau JH.** 2001. Modifier genes in mice and humans. *Nat Rev Genet* **2**:165-174.

- 844 40. **Collaborative Cross Consortium.** 2012. The genome architecture of the Collaborative
845 Cross mouse genetic reference population. *Genetics* **190**:389-401.
- 846 41. **Roberts A, Pardo-Manuel de Villena F, Wang W, McMillan L, Threadgill DW.**
847 2007. The polymorphism architecture of mouse genetic resources elucidated using
848 genome-wide resequencing data: implications for QTL discovery and systems genetics.
849 *Mamm Genome* **18**:473-481.
- 850 42. **Keane TM, Goodstadt L, Danecek P, White MA, Wong K, Yalcin B, Heger A, Agam**
851 **A, Slater G, Goodson M, Furlotte NA, Eskin E, Nellaker C, Whitley H, Cleak J,**
852 **Janowitz D, Hernandez-Pliego P, Edwards A, Belgard TG, Oliver PL, McIntyre RE,**
853 **Bhomra A, Nicod J, Gan X, Yuan W, van der Weyden L, Steward CA, Bala S,**
854 **Stalker J, Mott R, Durbin R, Jackson IJ, Czechanski A, Guerra-Assuncao JA,**
855 **Donahue LR, Reinholdt LG, Payseur BA, Ponting CP, Birney E, Flint J, Adams DJ.**
856 2011. Mouse genomic variation and its effect on phenotypes and gene regulation. *Nature*
857 **477**:289-294.
- 858 43. **Rasmussen AL, Okumura A, Ferris MT, Green R, Feldmann F, Kelly SM, Scott DP,**
859 **Safronetz D, Haddock E, LaCasse R, Thomas MJ, Sova P, Carter VS, Weiss JM,**
860 **Miller DR, Shaw GD, Korth MJ, Heise MT, Baric RS, de Villena FP, Feldmann H,**
861 **Katze MG.** 2014. Host genetic diversity enables Ebola hemorrhagic fever pathogenesis
862 and resistance. *Science* **346**:987-991.
- 863 44. **Gralinski LE, Ferris MT, Aylor DL, Whitmore AC, Green R, Frieman MB, Deming**
864 **D, Menachery VD, Miller DR, Buus RJ, Bell TA, Churchill GA, Threadgill DW,**
865 **Katze MG, McMillan L, Valdar W, Heise MT, Pardo-Manuel de Villena F, Baric**
866 **RS.** 2015. Genome Wide Identification of SARS-CoV Susceptibility Loci Using the
867 Collaborative Cross. *PLoS Genet* **11**:e1005504.

- 868 45. **Graham JB, Thomas S, Swarts J, McMillan AA, Ferris MT, Suthar MS, Treuting**
869 **PM, Ireton R, Gale M, Jr., Lund JM.** 2015. Genetic diversity in the collaborative cross
870 model recapitulates human West Nile virus disease outcomes. *MBio* **6**:e00493-00415.
- 871 46. **Graham JB, Swarts JL, Wilkins C, Thomas S, Green R, Sekine A, Voss KM, Ireton**
872 **RC, Mooney M, Choonoo G, Miller DR, Treuting PM, Pardo Manuel de Villena F,**
873 **Ferris MT, McWeeney S, Gale M, Jr., Lund JM.** 2016. A Mouse Model of Chronic
874 West Nile Virus Disease. *PLoS Pathog* **12**:e1005996.
- 875 47. **Green R, Wilkins C, Thomas S, Sekine A, Hendrick DM, Voss K, Ireton RC,**
876 **Mooney M, Go JT, Choonoo G, Jeng S, de Villena FP, Ferris MT, McWeeney S,**
877 **Gale M, Jr.** 2017. Oas1b-dependent Immune Transcriptional Profiles of West Nile Virus
878 Infection in the Collaborative Cross. *G3 (Bethesda)* **7**:1665-1682.
- 879 48. **Bottomly D, Ferris MT, Aicher LD, Rosenzweig E, Whitmore A, Aylor DL,**
880 **Haagmans BL, Gralinski LE, Bradel-Tretheway BG, Bryan JT, Threadgill DW, de**
881 **Villena FP, Baric RS, Katze MG, Heise M, McWeeney SK.** 2012. Expression
882 quantitative trait Loci for extreme host response to influenza a in pre-collaborative cross
883 mice. *G3 (Bethesda)* **2**:213-221.
- 884 49. **Elbahesh H, Schughart K.** 2016. Genetically diverse CC-founder mouse strains
885 replicate the human influenza gene expression signature. *Sci Rep* **6**:26437.
- 886 50. **Ferris MT, Aylor DL, Bottomly D, Whitmore AC, Aicher LD, Bell TA, Bradel-**
887 **Tretheway B, Bryan JT, Buus RJ, Gralinski LE, Haagmans BL, McMillan L, Miller**
888 **DR, Rosenzweig E, Valdar W, Wang J, Churchill GA, Threadgill DW, McWeeney**
889 **SK, Katze MG, Pardo-Manuel de Villena F, Baric RS, Heise MT.** 2013. Modeling
890 host genetic regulation of influenza pathogenesis in the collaborative cross. *PLoS Pathog*
891 **9**:e1003196.

- 892 51. **Lore NI, Iraqi FA, Bragonzi A.** 2015. Host genetic diversity influences the severity of
893 *Pseudomonas aeruginosa* pneumonia in the Collaborative Cross mice. *BMC Genet*
894 **16:106.**
- 895 52. **Zhang J, Malo D, Mott R, Panthier JJ, Montagutelli X, Jaubert J.** 2018.
896 Identification of new loci involved in the host susceptibility to *Salmonella Typhimurium*
897 in collaborative cross mice. *BMC Genomics* **19:303.**
- 898 53. **Durrant C, Tayem H, Yalcin B, Cleak J, Goodstadt L, de Villena FP, Mott R, Iraqi**
899 **FA.** 2011. Collaborative Cross mice and their power to map host susceptibility to
900 *Aspergillus fumigatus* infection. *Genome Res* **21:1239-1248.**
- 901 54. **Noll KE, Ferris MT, Heise MT.** 2019. The Collaborative Cross: A Systems Genetics
902 Resource for Studying Host-Pathogen Interactions. *Cell Host Microbe* **25:484-498.**
- 903 55. **Rossi SL, Tesh RB, Azar SR, Muruato AE, Hanley KA, Auguste AJ, Langsjoen RM,**
904 **Paessler S, Vasilakis N, Weaver SC.** 2016. Characterization of a Novel Murine Model
905 to Study Zika Virus. *Am J Trop Med Hyg* **94:1362-1369.**
- 906 56. **Dowall SD, Graham VA, Rayner E, Hunter L, Atkinson B, Pearson G, Dennis M,**
907 **Hewson R.** 2017. Lineage-dependent differences in the disease progression of Zika virus
908 infection in type-I interferon receptor knockout (A129) mice. *PLoS Negl Trop Dis*
909 **11:e0005704.**
- 910 57. **Srivastava A, Morgan AP, Najarian ML, Sarsani VK, Sigmon JS, Shorter JR,**
911 **Kashfeen A, McMullan RC, Williams LH, Giusti-Rodriguez P, Ferris MT, Sullivan**
912 **P, Hock P, Miller DR, Bell TA, McMillan L, Churchill GA, de Villena FP.** 2017.
913 Genomes of the Mouse Collaborative Cross. *Genetics* **206:537-556.**

- 914 58. **Scott JM, Lebratti TJ, Richner JM, Jiang X, Fernandez E, Zhao H, Fremont DH,**
915 **Diamond MS, Shin H.** 2018. Cellular and Humoral Immunity Protect against Vaginal
916 Zika Virus Infection in Mice. *J Virol* doi:10.1128/JVI.00038-18.
- 917 59. **Liang H, Yang R, Liu Z, Li M, Liu H, Jin X.** 2018. Recombinant Zika virus envelope
918 protein elicited protective immunity against Zika virus in immunocompetent mice. *PLoS*
919 *One* **13**:e0194860.
- 920 60. **Rutledge H, Aylor DL, Carpenter DE, Peck BC, Chines P, Ostrowski LE, Chesler**
921 **EJ, Churchill GA, de Villena FP, Kelada SN.** 2014. Genetic regulation of Zfp30,
922 CXCL1, and neutrophilic inflammation in murine lung. *Genetics* **198**:735-745.
- 923 61. **Mashimo T, Lucas M, Simon-Chazottes D, Frenkiel MP, Montagutelli X, Ceccaldi**
924 **PE, Deubel V, Guenet JL, Despres P.** 2002. A nonsense mutation in the gene encoding
925 2'-5'-oligoadenylate synthetase/L1 isoform is associated with West Nile virus
926 susceptibility in laboratory mice. *Proc Natl Acad Sci U S A* **99**:11311-11316.
- 927 62. **Govero J, Esakky P, Scheaffer SM, Fernandez E, Drury A, Platt DJ, Gorman MJ,**
928 **Richner JM, Caine EA, Salazar V, Moley KH, Diamond MS.** 2016. Zika virus
929 infection damages the testes in mice. *Nature* **540**:438-442.
- 930 63. **Manangeeswaran M, Ireland DD, Verthelyi D.** 2016. Zika (PRVABC59) Infection Is
931 Associated with T cell Infiltration and Neurodegeneration in CNS of Immunocompetent
932 Neonatal C57Bl/6 Mice. *PLoS pathogens* **12**:e1006004.
- 933 64. **van den Pol AN, Mao G, Yang Y, Ornaghi S, Davis JN.** 2017. Zika Virus Targeting in
934 the Developing Brain. *J Neurosci* **37**:2161-2175.
- 935 65. **Li S, Armstrong N, Zhao H, Hou W, Liu J, Chen C, Wan J, Wang W, Zhong C, Liu**
936 **C, Zhu H, Xia N, Cheng T, Tang Q.** 2018. Zika Virus Fatally Infects Wild Type
937 Neonatal Mice and Replicates in Central Nervous System. *Viruses* **10**.

- 938 66. **Gorman MJ, Caine EA, Zaitsev K, Begley MC, Weger-Lucarelli J, Uccellini MB,**
939 **Tripathi S, Morrison J, Yount BL, Dinnon KH, 3rd, Ruckert C, Young MC, Zhu Z,**
940 **Robertson SJ, McNally KL, Ye J, Cao B, Mysorekar IU, Ebel GD, Baric RS, Best**
941 **SM, Artyomov MN, Garcia-Sastre A, Diamond MS.** 2018. An Immunocompetent
942 Mouse Model of Zika Virus Infection. *Cell Host Microbe* **23**:672-685 e676.
- 943 67. **Manet C, Roth C, Tawfik A, Cantaert T, Sakuntabhai A, Montagutelli X.** 2018. Host
944 genetic control of mosquito-borne Flavivirus infections. *Mamm Genome* **29**:384-407.
- 945 68. **Samuel MA, Diamond MS.** 2005. Alpha/beta interferon protects against lethal West
946 Nile virus infection by restricting cellular tropism and enhancing neuronal survival. *J*
947 *Virol* **79**:13350-13361.
- 948 69. **Churchill GA, Airey DC, Allayee H, Angel JM, Attie AD, Beatty J, Beavis WD,**
949 **Belknap JK, Bennett B, Berrettini W, Bleich A, Bogue M, Broman KW, Buck KJ,**
950 **Buckler E, Burmeister M, Chesler EJ, Cheverud JM, Clapcote S, Cook MN, Cox**
951 **RD, Crabbe JC, Crusio WE, Darvasi A, Deschepper CF, Doerge RW, Farber CR,**
952 **Forejt J, Gaile D, Garlow SJ, Geiger H, Gershenfeld H, Gordon T, Gu J, Gu W, de**
953 **Haan G, Hayes NL, Heller C, Himmelbauer H, Hitzemann R, Hunter K, Hsu HC,**
954 **Iraqi FA, Ivandic B, Jacob HJ, Jansen RC, Jepsen KJ, Johnson DK, Johnson TE,**
955 **Kempermann G, et al.** 2004. The Collaborative Cross, a community resource for the
956 genetic analysis of complex traits. *Nat Genet* **36**:1133-1137.
- 957 70. **Duffy MR, Chen TH, Hancock WT, Powers AM, Kool JL, Lanciotti RS, Pretrick M,**
958 **Marfel M, Holzbauer S, Dubray C, Guillaumot L, Griggs A, Bel M, Lambert AJ,**
959 **Laven J, Kosoy O, Panella A, Biggerstaff BJ, Fischer M, Hayes EB.** 2009. Zika virus
960 outbreak on Yap Island, Federated States of Micronesia. *The New England journal of*
961 *medicine* **360**:2536-2543.

- 962 71. **Aliota MT, Caine EA, Walker EC, Larkin KE, Camacho E, Osorio JE.** 2016.
963 Characterization of Lethal Zika Virus Infection in AG129 Mice. *PLoS Negl Trop Dis*
964 **10:e0004682.**
- 965 72. **Dowall SD, Graham VA, Rayner E, Atkinson B, Hall G, Watson RJ, Bosworth A,**
966 **Bonney LC, Kitchen S, Hewson R.** 2016. A Susceptible Mouse Model for Zika Virus
967 Infection. *PLoS neglected tropical diseases* **10:e0004658.**
- 968 73. **do Valle TZ, Billecocq A, Guillemot L, Alberts R, Gomet C, Geffers R, Calabrese**
969 **K, Schughart K, Bouloy M, Montagutelli X, Panthier JJ.** 2010. A new mouse model
970 reveals a critical role for host innate immunity in resistance to Rift Valley fever. *J*
971 *Immunol* **185:6146-6156.**
- 972 74. **Le-Trilling VT, Trilling M.** 2017. Mouse newborn cells allow highly productive mouse
973 cytomegalovirus replication, constituting a novel convenient primary cell culture system.
974 *PLoS One* **12:e0174695.**
- 975 75. **Setoh YX, Peng NY, Nakayama E, Amarilla AA, Prow NA, Suhrbier A, Khromykh**
976 **AA.** 2018. Fetal Brain Infection Is Not a Unique Characteristic of Brazilian Zika Viruses.
977 *Viruses* **10.**
- 978 76. **Savidis G, Perreira JM, Portmann JM, Meraner P, Guo Z, Green S, Brass AL.**
979 2016. The IFITMs Inhibit Zika Virus Replication. *Cell Rep* **15:2323-2330.**
- 980 77. **Horisberger MA, Staeheli P, Haller O.** 1983. Interferon induces a unique protein in
981 mouse cells bearing a gene for resistance to influenza virus. *Proc Natl Acad Sci U S A*
982 **80:1910-1914.**
- 983 78. **Keele GR, Crouse WL, Kelada SNP, Valdar W.** 2019. Determinants of QTL Mapping
984 Power in the Realized Collaborative Cross. *G3 (Bethesda)* doi:10.1534/g3.119.400194.

- 985 79. **Simon-Loriere E, Lin RJ, Kalayanarooj SM, Chuansumrit A, Casademont I, Lin**
986 **SY, Yu HP, Lert-Itthiporn W, Chaiyaratana W, Tangthawornchaikul N,**
987 **Tangnararatchakit K, Vasanawathana S, Chang BL, Suriyaphol P, Yoksan S,**
988 **Malasit P, Despres P, Paul R, Lin YL, Sakuntabhai A.** 2015. High Anti-Dengue Virus
989 Activity of the OAS Gene Family Is Associated With Increased Severity of Dengue. *J*
990 *Infect Dis* **212**:2011-2020.
- 991 80. **Welsh CE, Miller DR, Manly KF, Wang J, McMillan L, Morahan G, Mott R, Iraqi**
992 **FA, Threadgill DW, de Villena FP.** 2012. Status and access to the Collaborative Cross
993 population. *Mamm Genome* **23**:706-712.
- 994 81. **Fansiri T, Fontaine A, Diancourt L, Caro V, Thaisomboonsuk B, Richardson JH,**
995 **Jarman RG, Ponlawat A, Lambrechts L.** 2013. Genetic mapping of specific
996 interactions between *Aedes aegypti* mosquitoes and dengue viruses. *PLoS Genet*
997 **9**:e1003621.
- 998 82. **Tokuda S, Do Valle TZ, Batista L, Simon-Chazottes D, Guillemot L, Bouloy M,**
999 **Flamand M, Montagutelli X, Panthier JJ.** 2015. The genetic basis for susceptibility to
1000 Rift Valley fever disease in MBT/Pas mice. *Genes Immun* **16**:206-212.
- 1001 83. **Sheehan KC, Lazear HM, Diamond MS, Schreiber RD.** 2015. Selective Blockade of
1002 Interferon-alpha and -beta Reveals Their Non-Redundant Functions in a Mouse Model of
1003 West Nile Virus Infection. *PloS one* **10**:e0128636.
- 1004 84. **Shimizu S.** 2004. CHAPTER 32 - Routes of Administration, p 527-542. *In* Hedrich HJ,
1005 Bullock G (ed), *The Laboratory Mouse* doi:[https://doi.org/10.1016/B978-012336425-](https://doi.org/10.1016/B978-012336425-8/50085-6)
1006 [8/50085-6](https://doi.org/10.1016/B978-012336425-8/50085-6). Academic Press, London.

- 1007 85. **Lanciotti RS, Kosoy OL, Laven JJ, Velez JO, Lambert AJ, Johnson AJ, Stanfield**
1008 **SM, Duffy MR.** 2008. Genetic and serologic properties of Zika virus associated with an
1009 epidemic, Yap State, Micronesia, 2007. *Emerg Infect Dis* **14**:1232-1239.
- 1010 86. **Faye O, Faye O, Diallo D, Diallo M, Weidmann M, Sall AA.** 2013. Quantitative real-
1011 time PCR detection of Zika virus and evaluation with field-caught mosquitoes. *Virology* **10**:311.
1012
- 1013 87. **Fontaine A, Jiolle D, Moltini-Conclois I, Lequime S, Lambrechts L.** 2016. Excretion
1014 of dengue virus RNA by *Aedes aegypti* allows non-destructive monitoring of viral
1015 dissemination in individual mosquitoes. *Sci Rep* **6**:24885.
- 1016 88. **Verdonk F, Roux P, Flamant P, Fiette L, Bozza FA, Simard S, Lemaire M, Plaud B,**
1017 **Shorte SL, Sharshar T, Chretien F, Danckaert A.** 2016. Phenotypic clustering: a novel
1018 method for microglial morphology analysis. *J Neuroinflammation* **13**:153.
- 1019 89. **Broman KW, Gatti DM, Simecek P, Furlotte NA, Prins P, Sen S, Yandell BS,**
1020 **Churchill GA.** 2019. R/qtl2: Software for Mapping Quantitative Trait Loci with High-
1021 Dimensional Data and Multiparent Populations. *Genetics* **211**:495-502.
1022
1023

1024

1025 **FIGURE LEGENDS**

1026 **FIG 1** ZIKV disease severity in *Ifnar1*-deficient mice is driven by the genetic background.

1027 6-7 week-old 129-*Ifnar1* (n = 7) and B6-*Ifnar1* (n = 10) mice were infected IP with 10^7 FFUs of
1028 ZIKV FG15 and monitored for 14 days. (A) Average clinical score, with numerical values given
1029 as follows: 0, no symptom; 1, ruffled fur; 2, emaciation, hunched posture and/or hypo activity; 3,
1030 hind limb weakness, prostration and/or closed eyes; and 4, moribund or dead. (B) Kaplan-Meier
1031 survival curves showing 100% lethality in B6-*Ifnar1* mice at day 7 p.i. and survival of 6/7 129-
1032 *Ifnar1* mice (logrank test, ***: p = 0.0002). B6-*Ifnar1* mice developed early symptoms which
1033 rapidly evolved to death, while 129-*Ifnar1* mice developed symptoms two days later which
1034 eventually resolved in most mice.

1035 **FIG 2** Establishment and validation of the experimental conditions for assessing susceptibility to
1036 ZIKV in CC strains. (A) The efficacy of the MAR1-5A3 mAb ($100\mu\text{g}$ for 5.10^6 cells) to block
1037 the IFNAR receptor in diverse mouse genetic backgrounds was determined by assessing STAT1
1038 phosphorylation by Western blotting on mouse embryonic fibroblasts (MEFs) derived from
1039 C57BL/6J, CC001, CC071 and CD-1 strains. (B) Plasma viral load measured on days 2, 3 and 6
1040 p.i. by RT-qPCR on 6-8 week-old mice of the CC001 and CC071 strains treated with MAR1-
1041 5A3 24h prior to ZIKV infection (filled circles; n = 9 and 8, respectively) or untreated (open
1042 circles; n = 3 and 2, respectively). "x" denotes a sample below the detection level. (C) Kinetics of
1043 plasma viral load in 129-*Ifnar1* and 4 CC strains measured by RT-qPCR. Each circle represents a
1044 6-8 week-old mouse analyzed on days 1, 2, 3 and 6. (D) Correlation between plasma viral load
1045 determined by FFA (x-axis) and RT-qPCR (y-axis) on 46 blood samples from 129-*Ifnar1*, B6-
1046 *Ifnar1* and 10 CC strains (circles show the mean of each strain; the number of 6-8 week-old mice

1047 per strain is shown in parentheses). (E) Plasma viral load measured by RT-qPCR at day 2 p.i. in
1048 6-8 week-old males and females of 129-*Ifnar1* and 4 CC strains for which both sexes had been
1049 tested (with $n \geq 4$ mice per group). (F) Effect of the dose of MAR1-5A3 antibody treatment on
1050 the rate of decrease of plasma viral load. 7-9 week-old mice of the CC012 and CC037 strains (4
1051 mice per group) received 2mg MAR1-5A3 mAb one day prior to being inoculated IP with 10^7
1052 FFUs of ZIKV FG15. The 4mg groups received additional IP injections of 1mg of mAb on days
1053 2 and 4 p.i. Plasma viral load was measured on days 2 and 6 p.i. (above and below by the dashed
1054 line, respectively).

1055 **FIG 3** CC genetic diversity strongly impacts clinical severity and plasma viral load. Thirty-five
1056 CC strains ($n = 2$ to 9, 6-8 week-old, mice per strain) were infected IP with 10^7 FFUs of ZIKV
1057 FG15, 24hr after IP injection of 2 mg of MAR1-5A3 mAb. 129-*Ifnar1* ($n = 24$) and B6-*Ifnar1* (n
1058 $= 5$) mice were similarly infected without mAb treatment. (A) Clinical scores at day 7 p.i. as the
1059 percentage of mice in the five levels of severity (same as in Fig. 1). (B) Plasma viral load at days
1060 2 (upper values) and 6 p.i. (lower values) quantified by RT-qPCR, shown as box-whisker plot
1061 with outliers as dots (strains are shown in the same order as in A). (C) Difference between
1062 plasma viral loads at days 2 and 6 p.i. Strains are sorted by increasing absolute difference,
1063 therefore in a different order from A and B. (B and C) Arrows indicate the subset of CC mouse
1064 strains selected for detailed study.

1065 **FIG 4** The differences in susceptibility to ZIKV between CC strains are conserved with other
1066 flaviviruses. (A) Six to 8 week-old mice from three selected CC strains treated with MAR1-5A3
1067 mAb and 129-*Ifnar1* mice were infected intraperitoneally with 10^3 FFUs of ZIKV HD78788.
1068 Left: average clinical score, with numerical values given as in Fig. 1. Center: Kaplan-Meier
1069 survival curves (logrank test). Right: plasma viral load at day 2 p.i., measured by RT-qPCR

1070 (Wilcoxon). (B) Viral load after ZIKV infection (left, data extracted from Fig. 3) and DENV
1071 infection (right, IV infection with $2 \cdot 10^6$ FFUs of DENV KDH0026A) was compared in mAb-
1072 treated CC001, CC071 and B6 6-8 week-old mice and in 129-*Ifnar1* and B6-*Ifnar1* (*t* test). (C)
1073 Left: Kaplan-Meier survival curves of four, 8-12 week-old, male mice of each of the three
1074 selected CC strains infected IP with 1000 FFU of WNV strain IS-98-ST1 and monitored for 14
1075 days (logrank test). Right: Kaplan-Meier survival curves of four to five, 8-12 week-old, male
1076 mice of BALB/cByJ and each of the three selected CC strains infected IP with 100 PFUs of
1077 RVFV strain ZH548 and monitored for 14 days (logrank test, $p > 0.05$). * $p < 0.05$; ** $p < 0.01$;
1078 *** $p < 0.001$.

1079 **FIG 5** Genetic analysis of susceptibility to ZIKV fails to identify simple genetic control.
1080 Genome-wide linkage analysis for the plasma viral load at day 2 p.i.(A), the plasma viral load at
1081 day 6 p.i. (B) and the decrease rate of plasma viral load (C) on the 35 CC strains shown on FIG
1082 3. The x-axis represents genomic location; the y-axis is the LOD score, representing the
1083 statistical association between the phenotype and the genomic location. Genome-wide thresholds
1084 $p = 0.1$, $p=0.05$ and $p = 0.01$, computed from 1000 permutations, are represented by dashed
1085 black, dashed red and plain red lines, respectively. No genome location reached the $p = 0.05$
1086 threshold.

1087 **FIG 6** Genetic variations between CC strains control brain viral load and histological profile in
1088 infected mice. Four to five, 6-8 week-old, mice of 129-*Ifnar1* and three selected CC strains were
1089 infected IP with 10^7 FFUs of ZIKV FG15 24hr after IP injection of 2 mg of MAR1-5A3 mAb.
1090 (A) Brain viral load measured by RT-qPCR at day 6 p.i. (Wilcoxon, *: $p < 0.05$). (B-N)
1091 Representative HE-stained brain sections at three different magnifications. (B-E) 129-*Ifnar1*
1092 mice (n=3). Black rectangle: encephalitis with perivascular lymphocyte cuffs; arrows: lesions of

1093 subacute leptomeningo-encephalitis. (F-H) CC001 mice (n=5). (I-K) CC005 mice (n=5). Black
1094 rectangle: encephalitis with perivascular lymphocyte cuffs; arrow: perivascular cuffing. (L-N)
1095 CC071 mice (n=4).

1096 **FIG 7** Genetic variations between CC strains control brain neuroinflammation in infected mice.
1097 Microglial reactivity was assessed on brain sections from the same mice as in Fig. 6 by anti-Iba1
1098 immunohistochemistry. (A) Quantification of Iba1 labeling signal on the brain sections (t tests; *
1099 $p < 0.05$; ** $p < 0.01$; *** $p < 0.001$). (B-M) Representative anti-Iba1 immunohistochemistry of
1100 brain sections at three different magnifications. (B-D) 129-*Ifnar1* mice (n=3), (E-G) CC001 mice
1101 (n=5), (H-J) CC005 mice (n=5), (K-M) CC071 mice (n=4). Arrowheads: nodules of activated
1102 microglial cells.

1103 **FIG 8** Intracranial ZIKV FG15 infection results in strain-dependent viral load and brain
1104 histological lesions. Groups of 5-6 week-old mice of 129-*Ifnar1* and three selected CC strains (3-
1105 5 mice per strain) were infected IC with 10^5 FFUs of ZIKV FG15 in the absence of prior anti-
1106 IFNAR treatment. (A) Brain viral load measured by RT-qPCR at day 6 p.i. (Wilcoxon, **: $p <$
1107 0.01). (B-O) Representative HE-stained brain sections at three different magnifications. (B-E)
1108 129-*Ifnar1* mice (n=4). Black rectangles: encephalitis with perivascular lymphocyte cuffs,
1109 arrows: leptomeningitis. (F-H) CC001 (n=5). (I-K) CC005 (n=4). (L-O) CC071 mice (n=5).
1110 Black rectangles: encephalitis with perivascular lymphocyte cuffs, arrows: leptomeningitis.

1111 **FIG 9** Intracranial ZIKV FG15 infection results in strain-dependent neuroinflammation of the
1112 brain. Microglial reactivity was assessed on brain sections from the same mice as in Fig. 8 by
1113 anti-Iba1 immunohistochemistry. (A) Quantification of Iba1 labeling signal on the brain sections
1114 (t tests; * $p < 0.05$; ** $p < 0.01$; *** $p < 0.001$). (B-M) Representative anti-Iba1
1115 immunohistochemistry of brain sections at three different magnifications. (B-D) 129-*Ifnar1* mice



1116 (n=4), (E-G) CC001 mice (n=5), (H-J) CC005 mice (n=4), (K-M) CC071 mice (n=5).




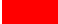
1117 Arrowheads: nodules of activated microglial cells.

1118 **FIG 10** Enhanced ZIKV replication in CC071 MEFs compared with CC001. MEFs derived from
1119 CC001 (blue) and CC071 (red) embryos were infected with ZIKV FG15 at MOI 5. ZIKV titer in
1120 the supernatant was quantified by focus-forming assay at 24, 48 and 72 hours p.i. Mean +/- SEM
1121 from 3 biological replicates. Results were replicated in 3 independent experiments. (t tests; ***
1122 $p < 0.001$).

1123

Strain	<i>Oas1b</i>	<i>Ifnar1</i>
CC001	B	F
CC002	A	B
CC003	H	B
CC004	G	B
CC005	B	E
CC006	E	D
CC007	D	B
CC009	E	D
CC011	B	G
CC012	H	A
CC013	E	E
CC017	H	D
CC018	D	C
CC019	H	C
CC021	C	D
CC024	E	A
CC025	H	A
CC026	A	H
CC027	B	G
CC032	B C *	B
CC037	B	C
CC039	H	B
CC040	B D *	D
CC041	F	D
CC042	H	F
CC043	C	C
CC045	C	H
CC049	B D *	D
CC051	E	B
CC059	E	B
CC060	D	F
CC061	E	A
CC068	B	E G *
CC071	C	F
CC072	C	D

functional 
 not functional 

 A/J allele
 B6 allele or identical
 CAST allele
 PWK allele

1124 * heterozygous strain

1125 A: A/J; B: C57BL/6J; C: 129S1/SvImJ; D: NOD/ShiLtJ; E: NZO/HILtJ; F: CAST/EiJ; G: PWK/PhJ; H: WSB/EiJ

1126 Data from <http://csbio.unc.edu/CCstatus/CCGenomes/#genotypes>.

1127 **Table 1. Origin of *Oas1b* and *Ifnar1* alleles in the 35 CC strains tested.**

1128

Position*	dbSNP	Reference (B6)	I29S1/SvImJ	A/J	CAST/EiJ	NOD/ShiLtJ	NZO/HILtJ	PWK/PhJ	WSB/EiJ	Amino acid	AA change**
91,485,366	rs235809125	C	-	-	T	-	-	-	-	8	A -> V
91,485,368	rs255866699	G	-	-	A	-	-	-	-	9	A -> T
91,499,433	rs31418313	G	-	A	-	-	-	-	-	274	R -> H
91,499,468	rs223171563	A	-	-	G	-	-	-	-	286	N -> D
91,499,532	rs240163845	A	-	-	G	-	-	G	-	307	H -> R
91,501,623	rs263194450	T	-	-	G	-	-	G	-	376	I -> R
91,501,631	rs246470801	G	-	-	A	-	-	A	-	379	E -> K
91,505,284	rs219805193	C	-	-	T	-	-	-	-	549	A -> V

1129 * positions 16:91,485,344-91,505,411 retrieved from the Sanger Institute Mouse Genomes Project
1130 (https://www.sanger.ac.uk/sanger/Mouse_SnpViewer/rel-1505)

1131 ** amino-acid changes compared with the reference (B6) sequence (CCDS database :
1132 <https://www.ncbi.nlm.nih.gov/CCDS/>)

1133

1134 **Table 2. Variants in the coding sequence of the *Ifnar1* gene.**

1135

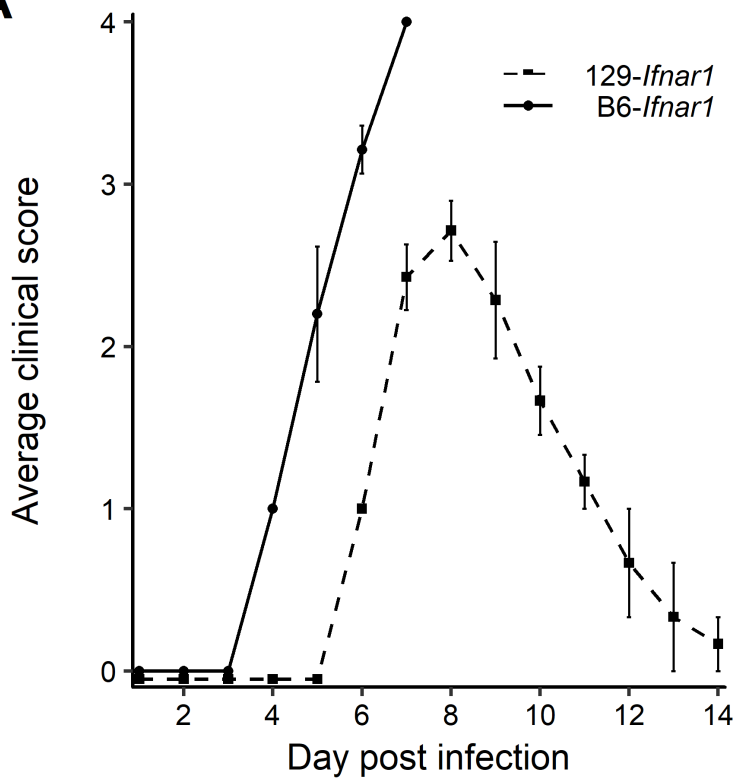
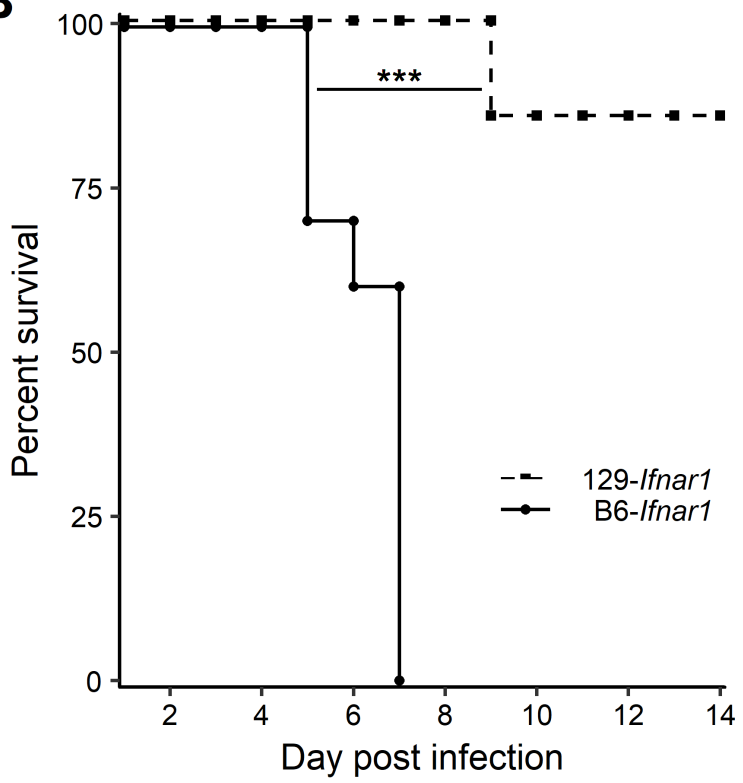
1136

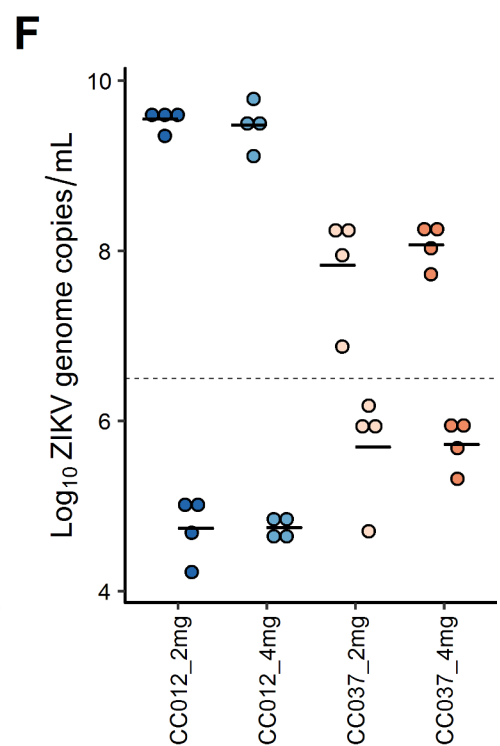
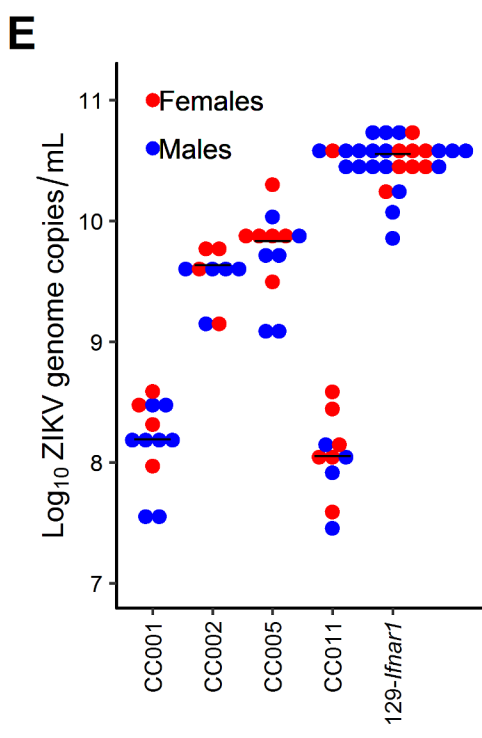
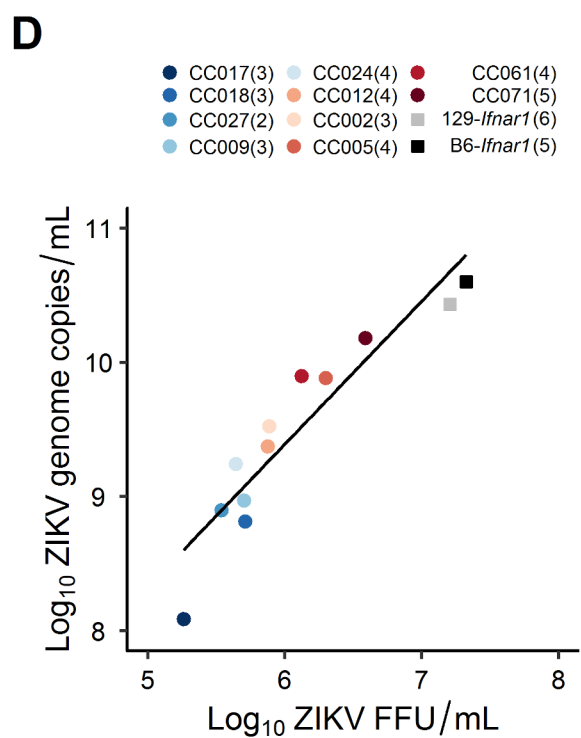
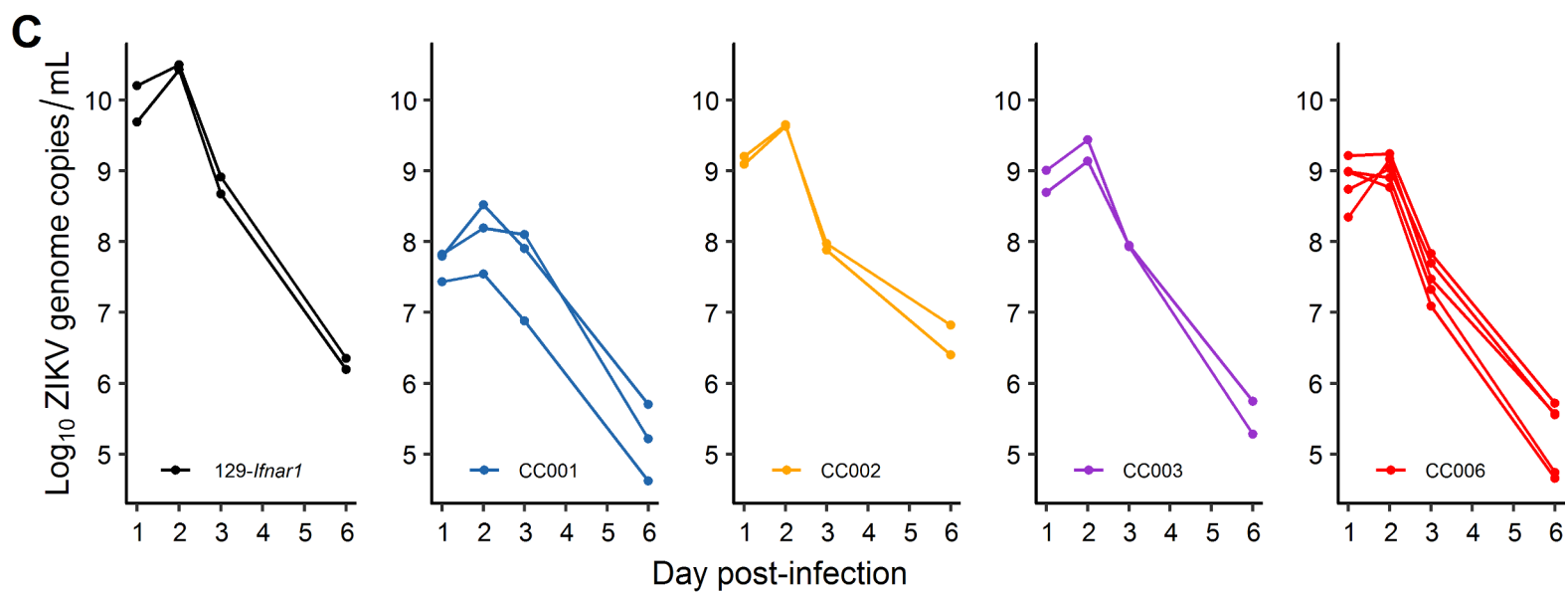
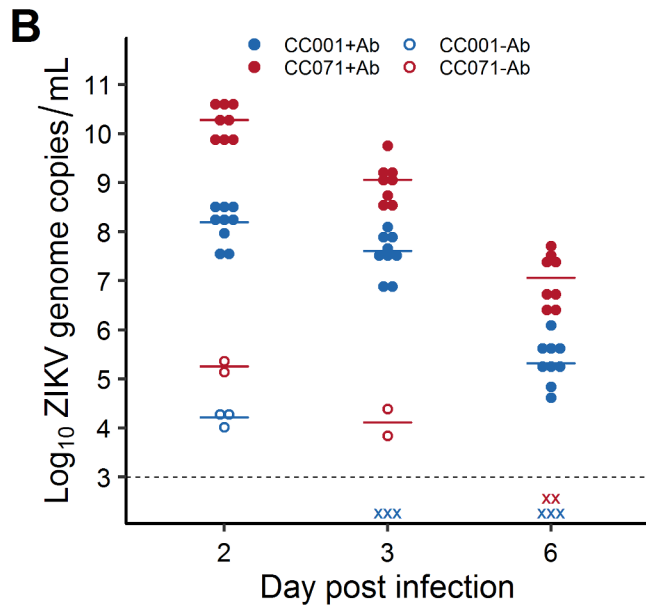
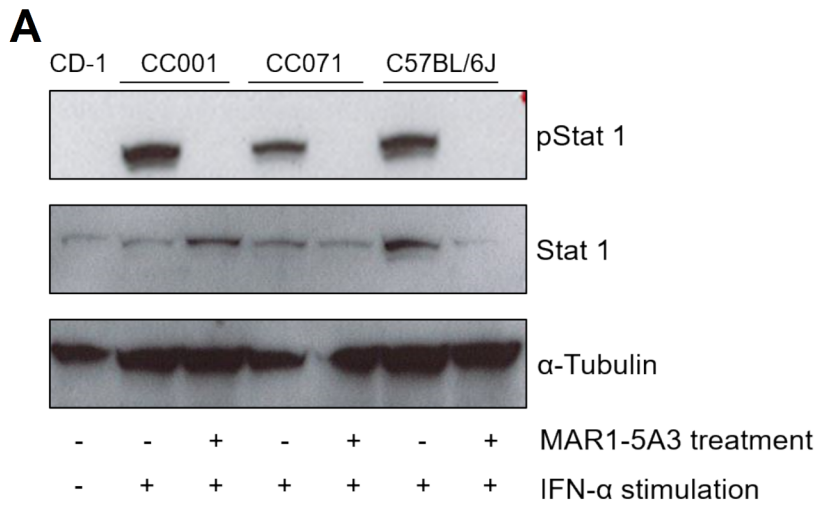
1137

	CC001	CC005	CC071	129- <i>Ifnar1</i>
Symptoms	—	—	+	+
Mortality	0%	0%	78%	12.5%
Peak plasma viral load	+	+	+	+
Rate of decrease of plasma viral load	↘	↓	↘	↓
Brain viral load (systemic infection)	+	+	+	+
Brain pathology (systemic infection)	—	+	+	+
Brain viral load (intracerebral infection)	+	+	+	+
Brain pathology (intracerebral infection)	+	+	+	+
Viral replication in vitro (24-72 hours)	↘	-	↗	-

1138

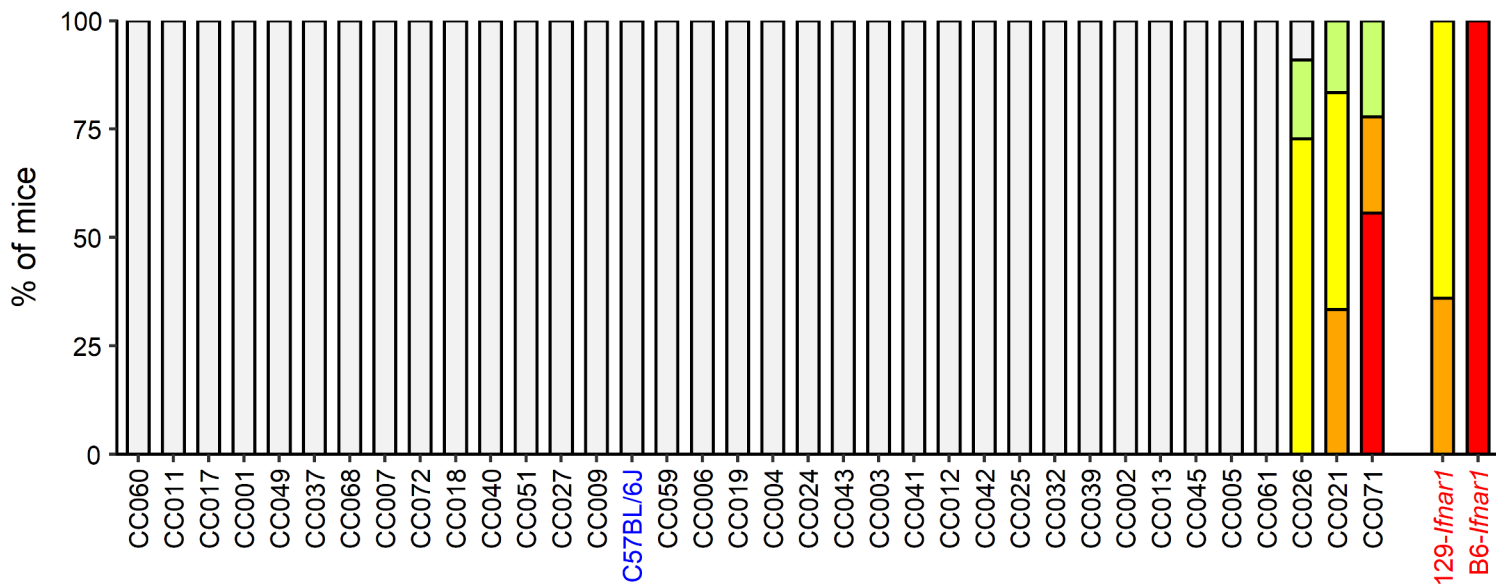
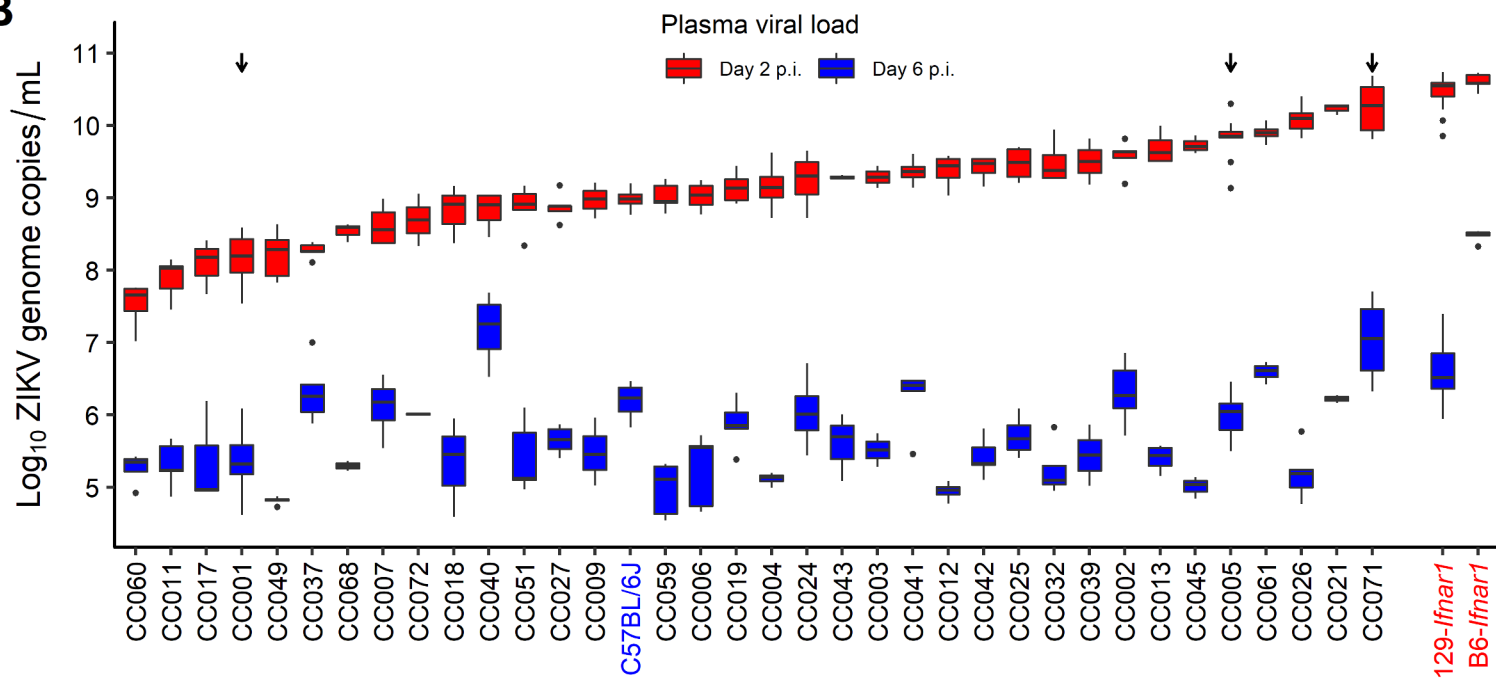
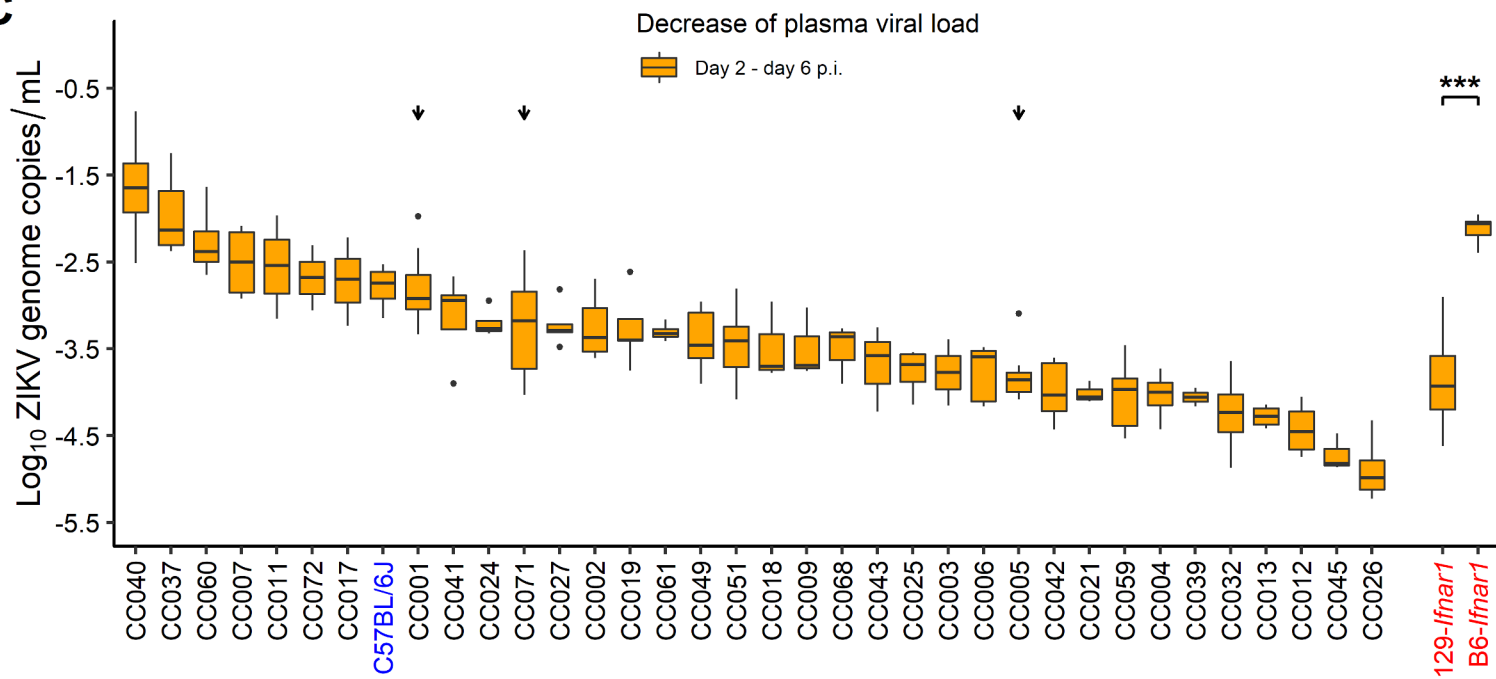
1139 **Table 3. Summary of the main features of ZIKV infection in mAb-treated CC strains and**
 1140 **129-*Ifnar1* mice.**

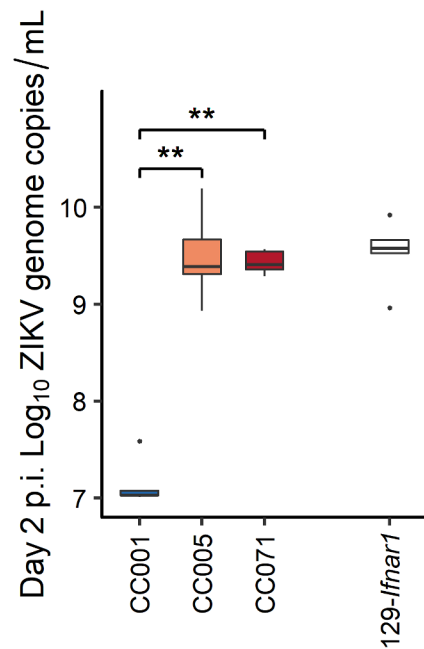
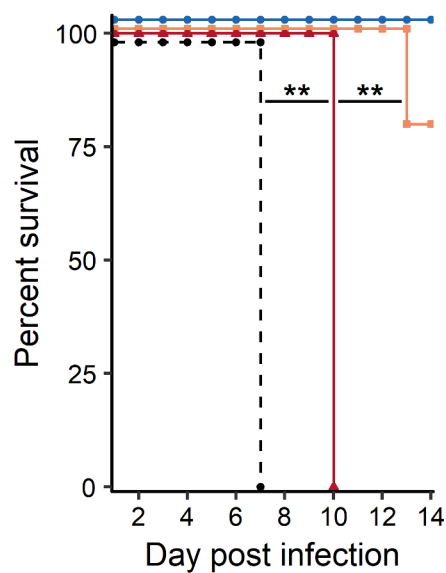
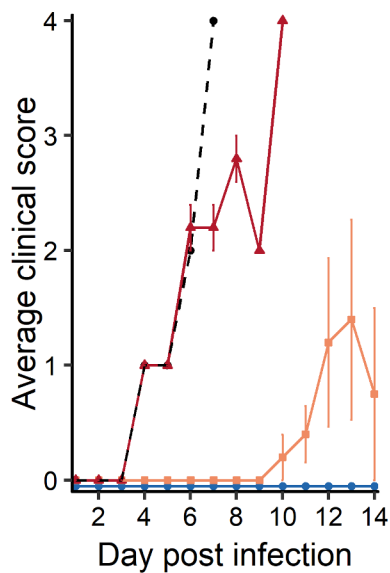
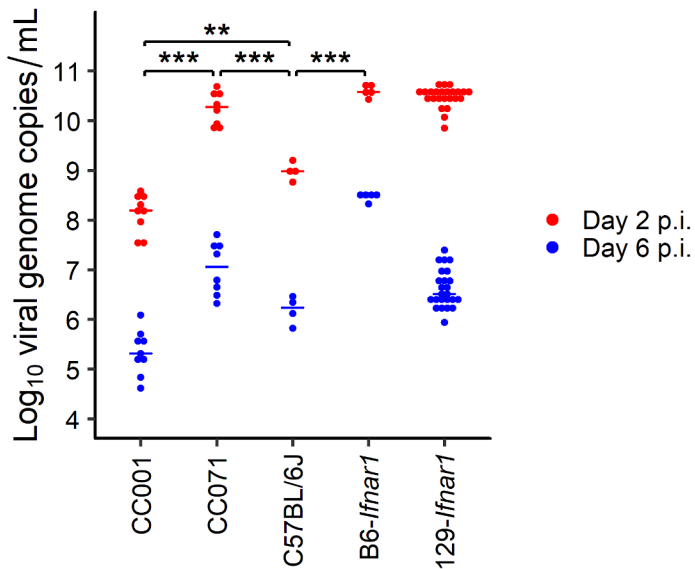
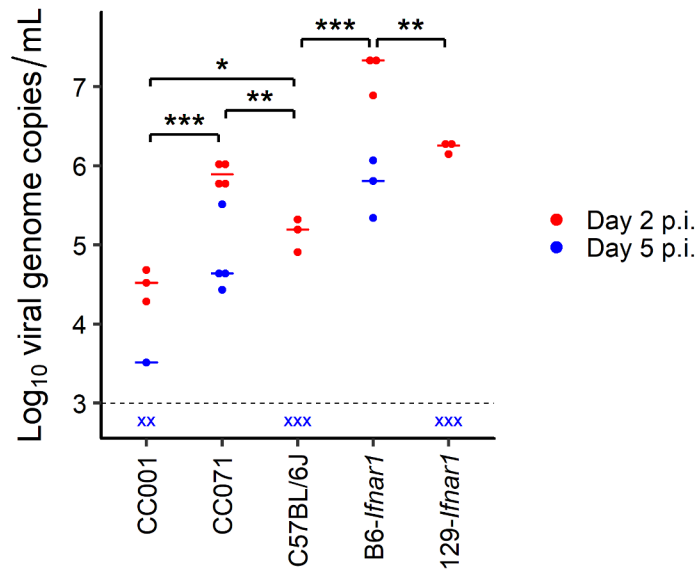
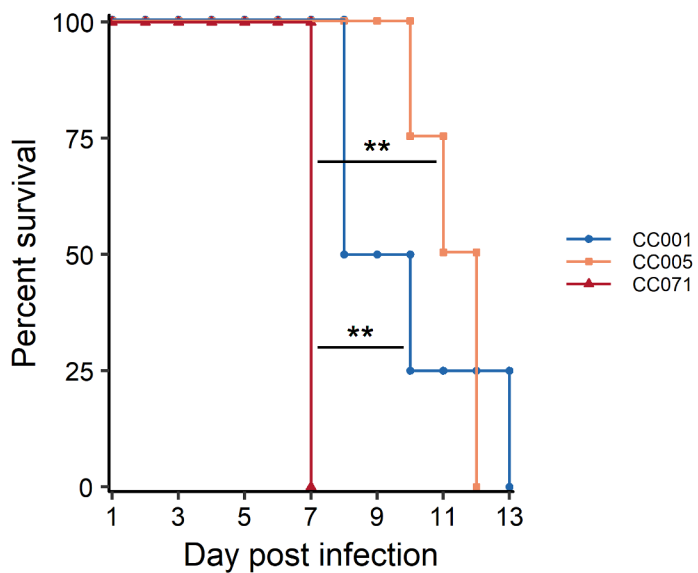
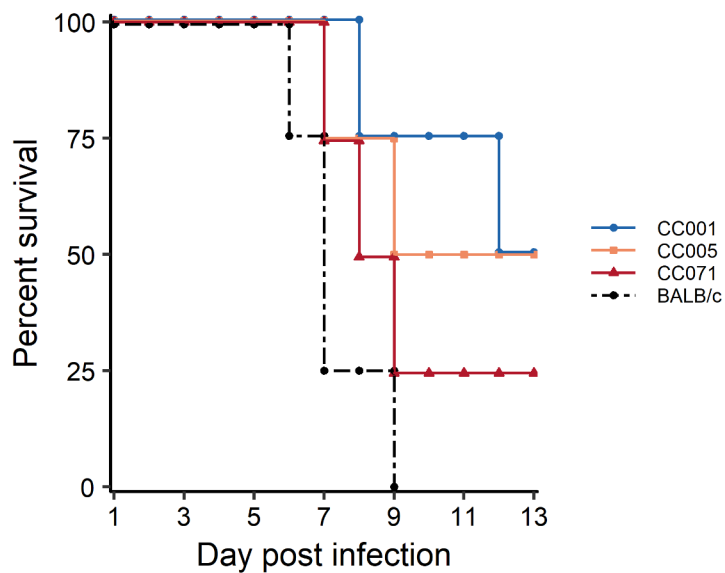
A**B**

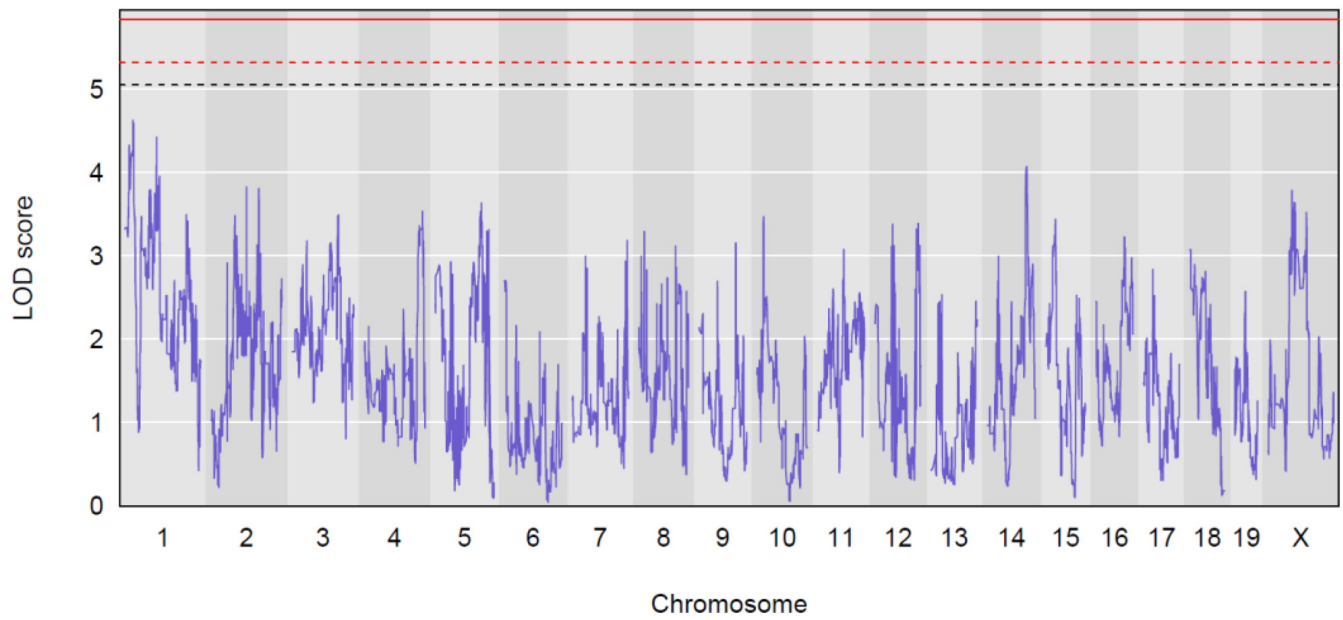
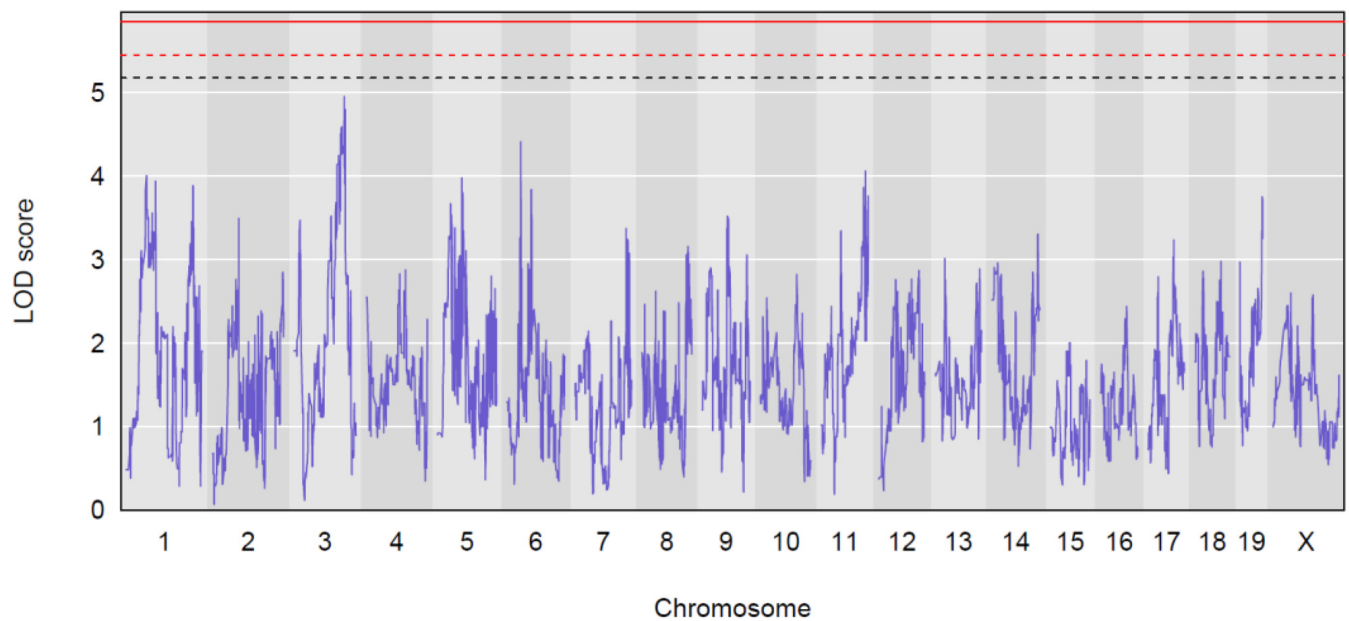
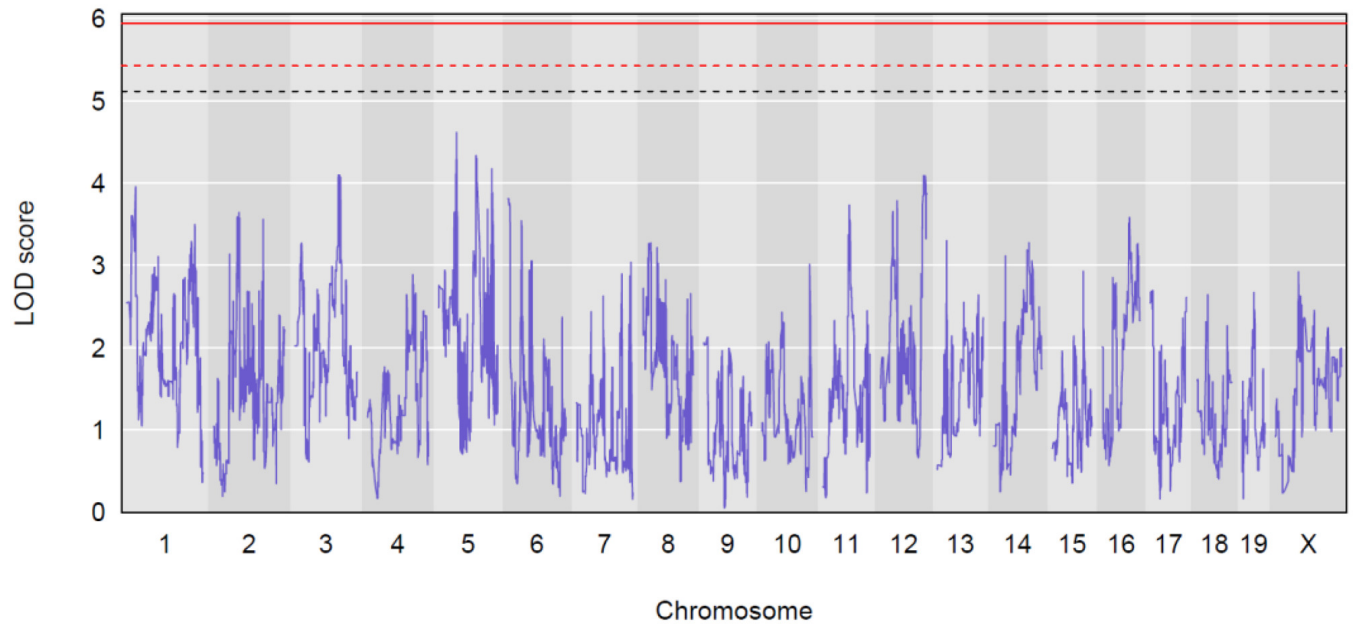


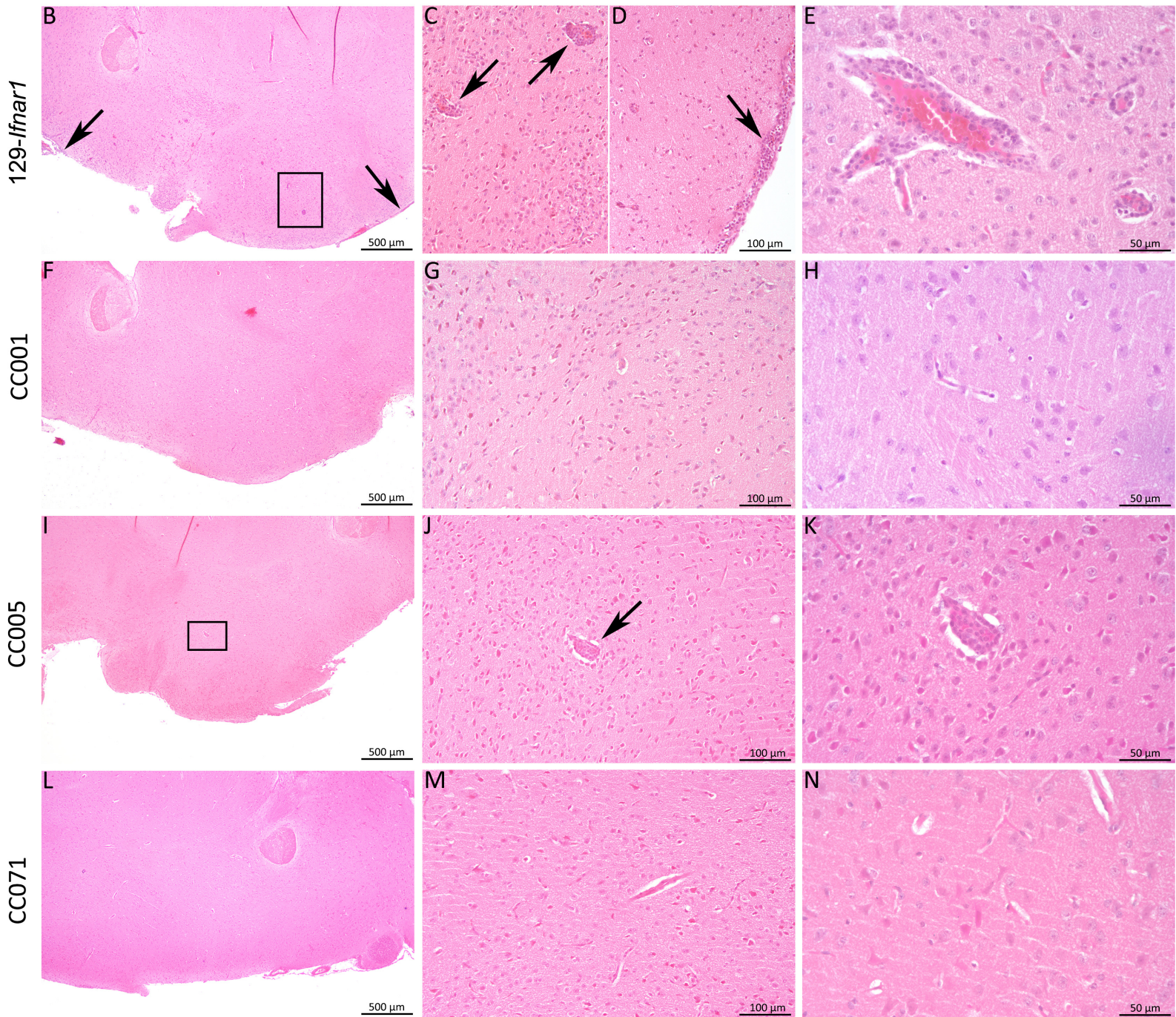
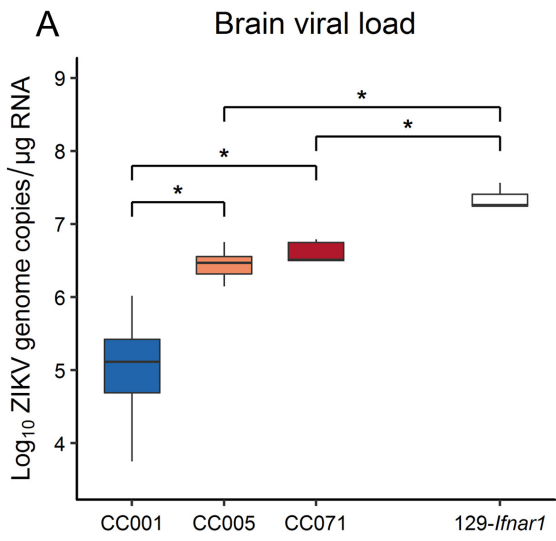
A

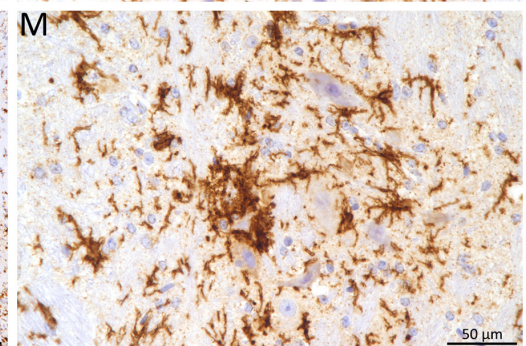
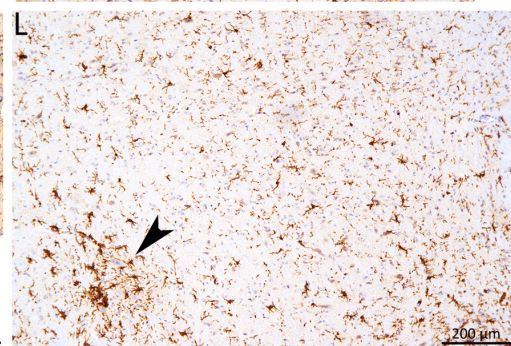
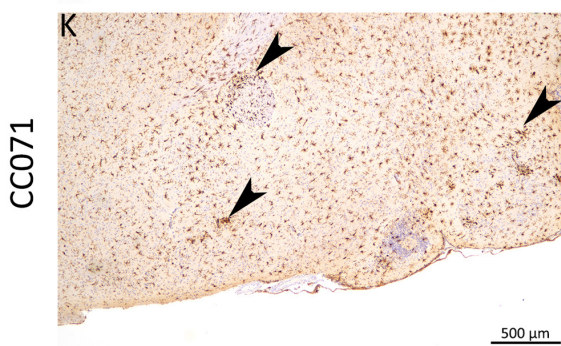
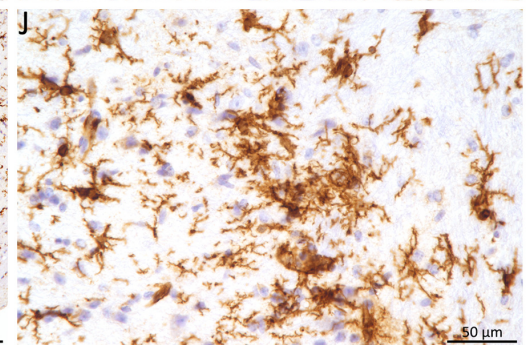
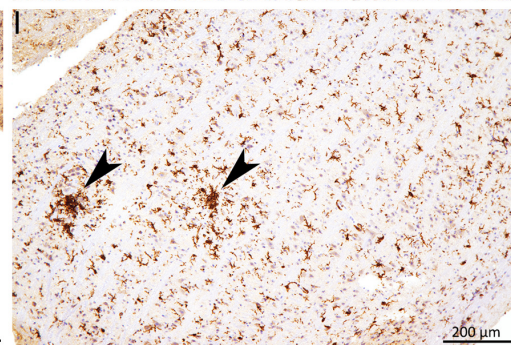
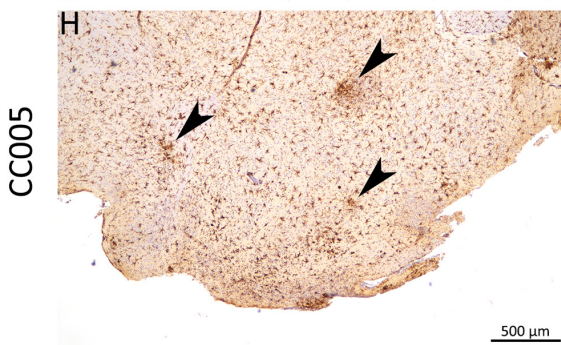
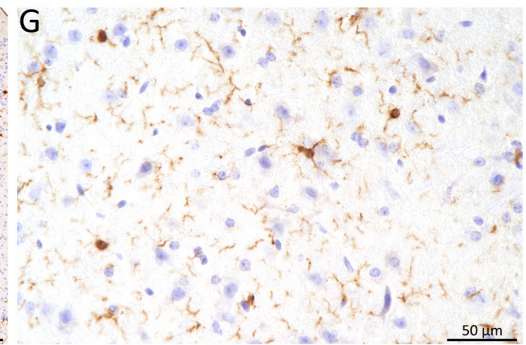
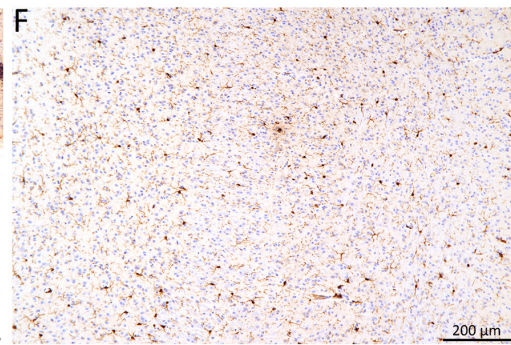
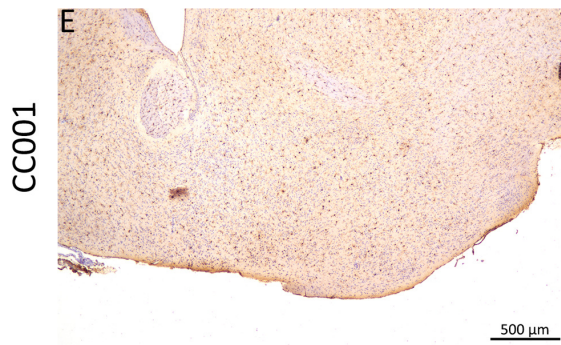
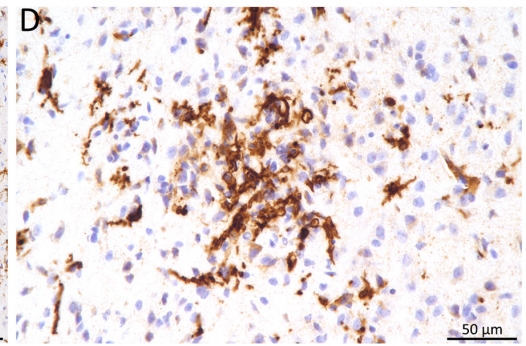
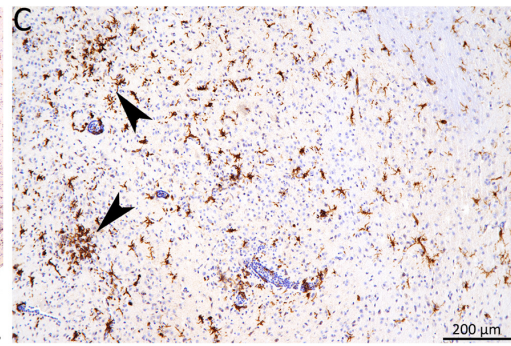
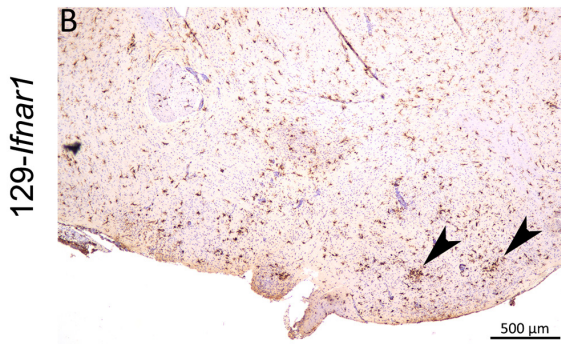
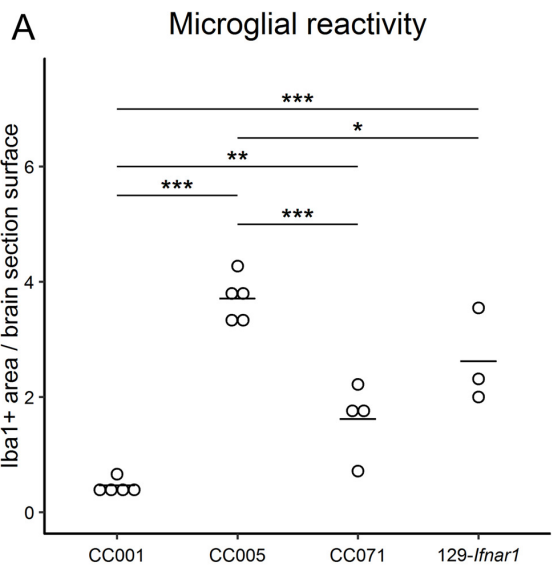
Clinical score at day 7 p.i. 0 1 2 3 4

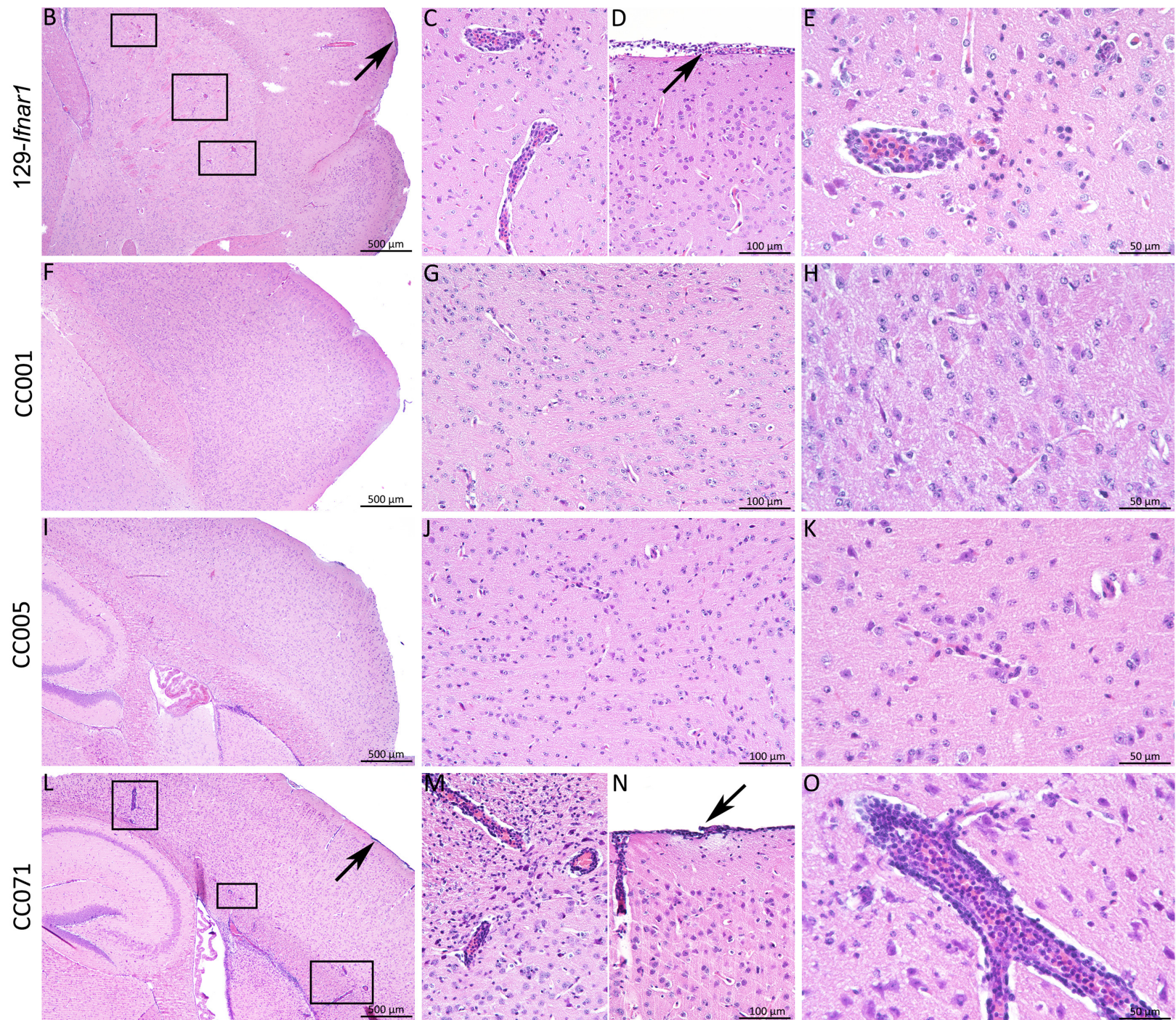
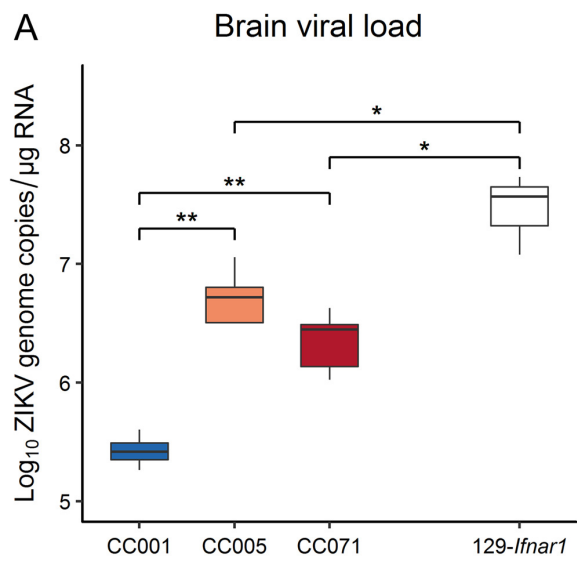
**B****C**

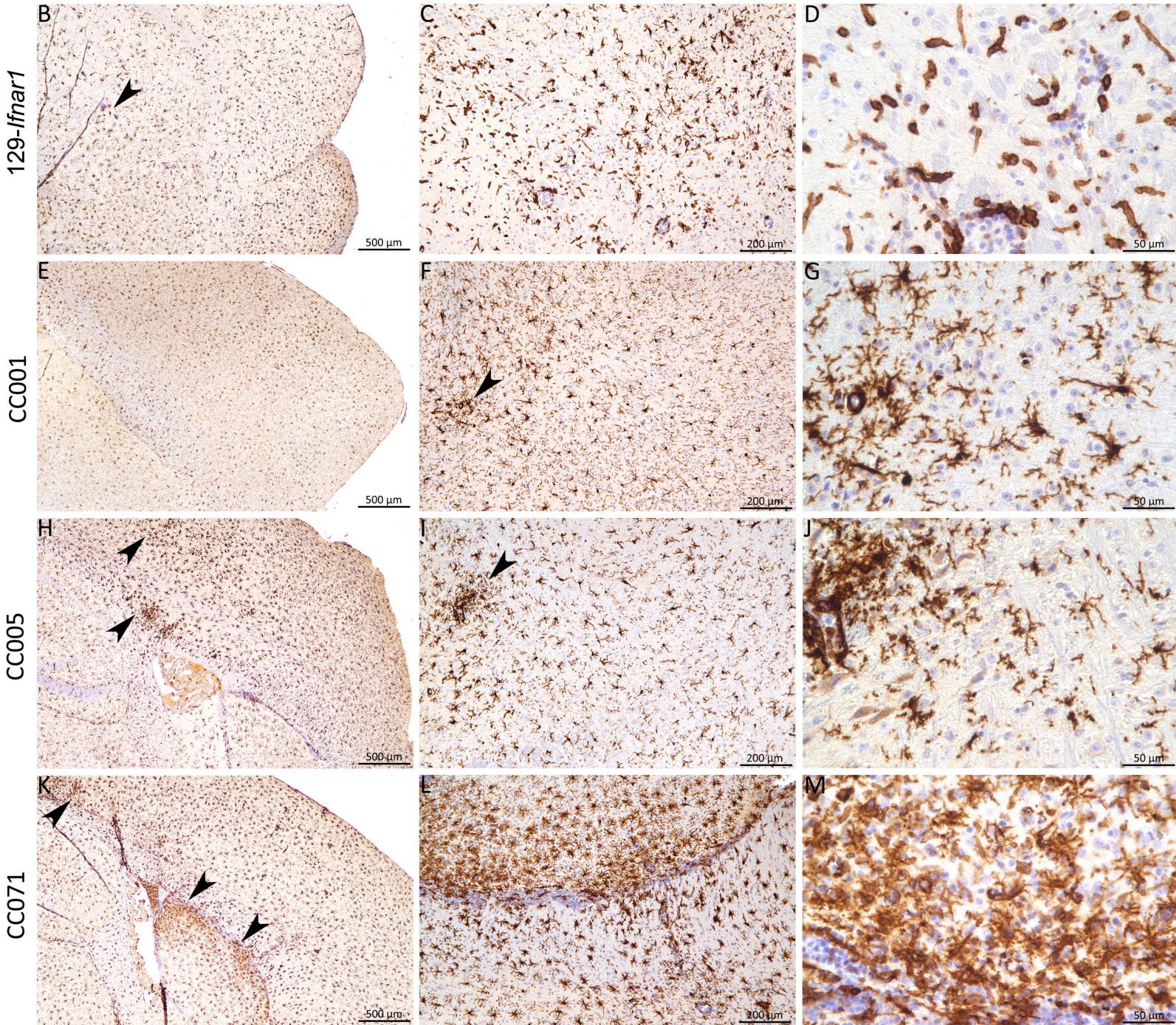
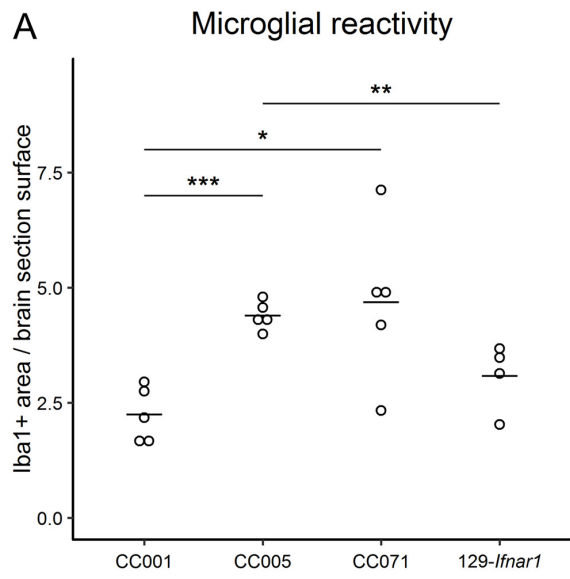
A**ZIKV HD78788****B****ZIKV****DENV****C****WNV****RVFV**

A**Day 2 : Plasma viral load****B****Day 6 : Plasma viral load****C****Day 2 - 6 : Decrease rate of plasma viral load**









Embryonic fibroblasts

CC001 CC071

